ULTRA WIDE BAND SIGNAL MODELING FOR RADAR RECEIVER CHARACTERIZATION

THESIS

Robert J. Backscheider, Second Lieutenant, USAF

AFIT/GE/ENG/04-28

DEPARTMENT OF THE AIR FORCE
AIR UNIVERSITY

AIR FORCE INSTITUTE OF TECHNOLOGY

Wright-Patterson Air Force Base, Ohio

The views expressed in this thesis are those of the author and do not reflect the official policy or position of the United States Air Force, Department of Defense, or the U.S. Government

AFIT/GE/ENG/04-28

ULTRA WIDE BAND SIGNAL MODELING FOR RADAR RECEIVER CHARACTERIZATION

THESIS

Presented to the Faculty

Department of Electrical and Computer Engineering

Graduate School of Engineering and Management

Air Force Institute of Technology

Air University

Air Education and Training Command

In Partial Fulfillment of the Requirements for the

Degree of Master of Science in Electrical Engineering

Robert J. Backscheider, BSEE

Second Lieutenant, USAF

December 2004

AFIT/GE/ENG/04-28

ULTRA WIDE BAND SIGNAL MODELING FOR RADAR RECEIVER CHARACTERIZATION

Robert J. Backscheider, BSEE

Second Lieutenant, USAF

Approved:

//signed//	9 December 2004
Dr. Michael A. Temple Thesis Advisor	Date
//signed//	2 December 2004
Dr. John F. Raquet Committee Member	Date
//signed//	9 December 2004
Major Todd B. Hale, PhD Committee Member	Date

Acknowledgments

I am grateful for the many that made this effort possible. Dr. Temple, thank you for your amazing patience and inspiration.

Robert J. Backscheider

Table of Contents

List of Figures

Page

List of Tables

Page

Abstract

Results for modeling, simulation, and analysis of interference effects that modern wideband signals have on existing narrowband radar system performance are presented. In particular, radar detection performance is characterized using a basic radar receiver model and operational parameters *consistent* with those of the ARSR-4 air route surveillance radar. Two modern wideband signals (interferers) are addressed in this work, including the GPS military signal (M-Code signal) and a direct sequence ultra wideband (DS-UWB) waveform meeting outdoor emission restrictions imposed by the Federal Communications Commission (FCC). Interference effects are characterized for an unmodulated sinusoidal pulse, as well as, linear frequency modulated (LFM) and bi-phase Barker coded pulse compression waveforms. Finally, coherent pulse integration is addressed and interference mitigation demonstrated via improved detection performance. Worst case detection scenarios from the radar's perspective are considered for all cases. M-Code interference results indicate that at proposed received power levels of −160 to −130 dBW, radar detection performance is severely degraded with expected improvement occurring when pulse integration is employed. DS-UWB interference results indicate that at maximum transmit power levels specified by the FCC, the DS-UWB waveform has minimal impact on detection performance for radar receiver/UWB transmitter separation distances beyond 0.5 meters. This separation distance is reduced further when pulse integration is employed.

ULTRA WIDE BAND SIGNAL MODELING FOR RADAR RECEIVER CHARACTERIZATION

I. Introduction

1.1 Background

This work provides modeling, simulation and analysis of interference effects that modern wideband signals (communication, navigation, etc.) have on existing radar system performance. Specifically, radar detection performance (robustness and/or degradation thereof) is characterized using a basic monostatic radar receiver model and operational parameters *consistent* with those of a deployed air route surveillance radar system (the ARSR-4 system).

Interference effects are characterized using an unmodulated sinusoidal pulse, a linear frequency modulated (LFM) pulse and a Barker phase coded pulse. Coherent pulse integration is also incorporated and interference power mitigation is demonstrated. For all cases considered, a worst case detection scenario (from the radar receiver perspective) is considered whereby relative radar and interferer locations are chosen such that minimum radar return power is received. Noise power is then adjusted to maintain the desired, fixed probability of false alarm (P_{FA}). Interfering power levels are next varied and the probability of detection (P_D) is determined.

Two modern wideband signals (interferers) are specifically addressed in this work, including the GPS military signal (M-Code signal) [1] and a direct sequence ultra

wideband (DS-UWB) waveform [2] which meets outdoor transmission specifications imposed by the Federal Communications Commission (FCC) rulings [3].

All M-Code results presented in this work are provided by way of validating the simulation performance obtained by Wruck [6], including the data in Section 2.2 and Section 3.3.

1.1.1 Modern GPS M-Code Signal

As the DoD's executive agent, the Air Force successfully developed and fielded the Global Positioning System (GPS), which provided initial operational capability in December 1993 [1]. Increased interest and use throughout military and civilian communities has dictated GPS modernization which increases received GPS signal power levels by as much as 20 dB [4].

At these power levels, the proposed GPS signals are approaching the 'typical' thermal noise floor of -201 dBW [5] (noise floor levels are a function of receiver noise temperature and vary between -206 dBW and -200 dBW). This decreased distance between the thermal noise floor and the GPS signal power has caused some concern within the aviation community that the new GPS military signal (M-Code) may interfere with existing radars.

Current GPS systems operate on two frequencies: 1575.42 MHz (designated L1) and 1227.6 MHz (designated L2). Two spread-spectrum Binary Phase Shift Keyed (BPSK) modulated signals are on the L1 frequency band. The first is the Precise (P)-code, which has a chipping rate of 10.23 MHZ, and the second is the Coarse/Acquisition (C/A)-code, which has a chipping rate of 1.023 MHz. The P-code is encrypted to provide

anti-spoofing (AS) capability and is denoted P(Y)-code. The C/A code is unencrypted and is used by all receivers to accomplish initial signal acquisition. For civilian applications, the C/A code is the only signal available for positioning. For military applications, the C/A code is used for acquisition prior to using the encrypted P(Y) –code for positioning. The P(Y) -code is currently the only signal transmitted on the L2 frequency band [6].

Since most of the L-band frequency spectrum is currently being used (L-band is well-suited for propagating radio signals from space), GPS modernization plans dictate the reuse of currently assigned frequency bands. In addition, the technical limitations and costs associated with modifying satellites to transmit at frequencies other than L1 and L2 are prohibitive [9]. Thus, the modernization plan involves 1) reusing the current L1 and L2 frequency bands while adding one new civilian signal on L2 and 2) adding a new signal at 1176.45 MHz (designated L5). The new M-Code signal will be placed on both L1 and L2 resulting in the structure shown in Fig. 1.1 [6].

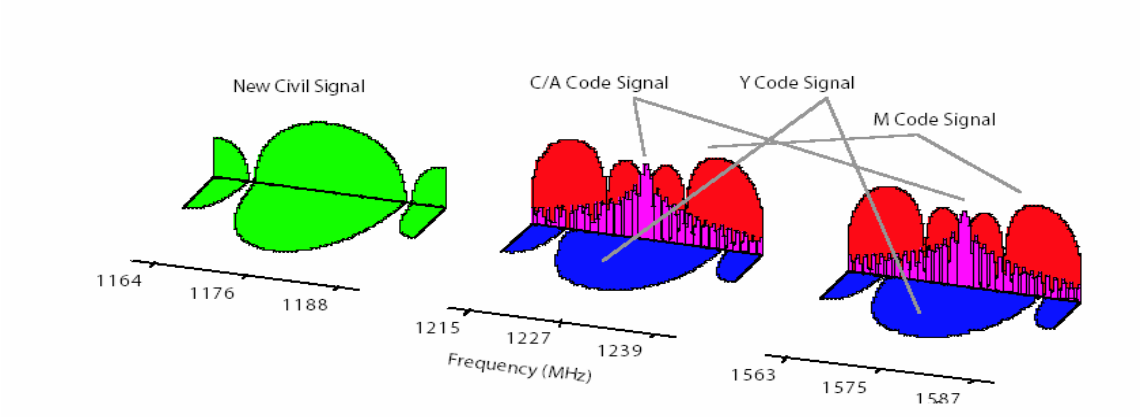

Figure 1.1: Modernized GPS Signal Architecture Showing M-Code [10].

1.1.2 Modern UWB Signals

In just over two years since being authorized [11], research and development on the unlicensed use of UWB communication devices operating in the 3.1 to 10.6 GHz band has exploded. The renewed interest in impulse-like signaling has spawned much research seeking to provide better communication capability (increased throughput, enhanced interference suppression, etc.) while being mindful of coexistence and collateral interference issues commonly encountered when introducing new technologies. Although the large bandwidth and relatively low power spectral densities authorized for UWB operation inherently provide some level of collateral interference suppression, the actual impact of UWB signaling on coexisting narrowband systems cannot be ignored [12, 13]. This work focuses on Gaussian monocycles and direct sequence time hopping techniques to provide UWB communication capability. Although time hopping techniques are fundamental to communication systems, the conceptual extension of time modulated (periodic displacement of a fundamental waveform shape) into radar systems is relatively natural. Thus, the broadband structured spectral responses seen in UWB communication signals are not that dissimilar from those obtained in UWB radar applications employing the same fundamental waveforms, e.g., the Gaussian monocycles [24].

The FCC defines an Ultra Wide Band waveform as one having a bandwidth greater than 500 MHz or a fractional bandwidth greater than twenty percent. Fractional bandwidth is measured at the -10 dB points and is defined as

$$B_{Frac} = 2 \cdot \frac{f_H - f_L}{f_H + f_L} \tag{1.1}$$

where f_H is the high frequency limit and f_L is the low frequency limit with respect to the center frequency. Figure 1.2 illustrates the FCC's definition of UWB. Gaussian monocycles are a class of UWB waveforms offering large bandwidths. The fundamental UWB waveform is modeled in this work as the second derivative of a Gaussian impulse to account for the effects of both the transmit and receive antennas. Figure 1.3 shows an example of the UWB waveform [2].

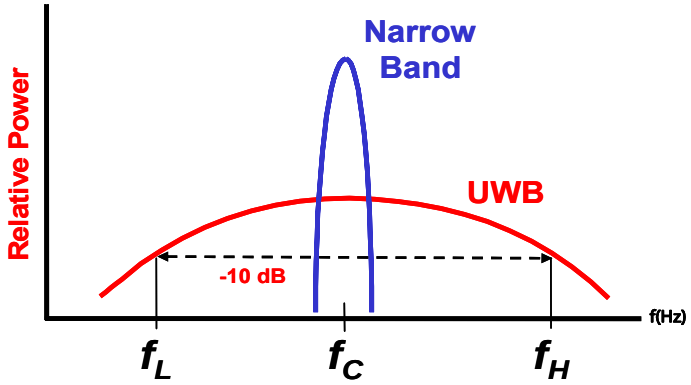

Figure 1.2: Illustration of UWB and Fractional Bandwidth [2]

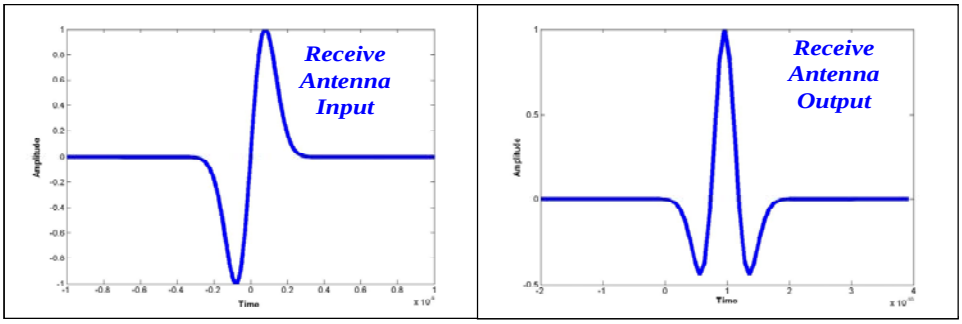

Figure 1.3: Fundamental UWB Waveform (Input and Output) [2]

1.2 Problem Statement

The purpose of this work is to model and simulate the effects (if any) that each of the modern signals described above may have on radar detection performance. The aviation community has expressed some concern that the new M-Code signal may interfere given its increased power levels and spectral location near the L2 frequency band. Furthermore, because of the wide operating bandwidths, UWB devices are operating in (or across) frequency bands allocated to both U.S. Government and non-government operations [2]. Thus, the FCC has requested that parties performing interference tests consider and provide information on receiver susceptibility to UWB signals, including spatial geometries assumed for evaluating potential interference [2].

1.3 Summary of Current Knowledge

Many studies have been conducted to examine the effects of external interference on GPS itself, with fewer conducted to ascertain the effect that GPS signals may have on other applications. Although current GPS signal power is sufficiently low such that minimal interference is occurring to most other systems, the proposed GPS modernization plan calls for higher M-Code power levels which may increase interference to coexisting systems.

Although unlicensed UWB devices are authorized to operate at low power levels, levels which have ideally been established to minimize interference to other systems, it is desirable to characterize an existing system's capability with UWB signals present. Likewise, current testing on UWB interference effects are not sufficient since the FCC

suggests that more analysis is needed to properly adjust emissions limitations for UWB devices to ensure such devices do not interfere with existing systems.

1.4 Scope

As stated in Section 1.2, the new M-Code is to be transmitted in the L1 and L2 band and is designed to coexist with the new civil signal and legacy P(Y)-code. Only the L2 band is considered during the M-Code characterization and analysis portion of this research because that is the frequency band in which the ARSR-4 operates. The worst case scenario (from the radar receiver perspective) for the UWB interferer occurs when the UWB power spectral density peak coincides with the radar's carrier frequency. For this work, this peak interfering condition occurs when the UWB signal is centered at 7.0 GHz for the Bi-Orthogonal Pulse Position Modulation (BPPM) waveform considered. Thus, this is the spectral region analyzed for the UWB interferer.

The radar system is initially modeled as a single pulse radar having no waveform coding for compression and no pulse integration for processing gain. For subsequent simulations, pulse compression and integration are introduced as commonly employed in fielded systems.

For all M-Code analyses, the target is assumed stationary at the maximum detectable range on radar bore sight. Furthermore, the target is co-aligned with a stationary GPS satellite which is also positioned along the radar bore sight. In all UWB analyses, the target is again assumed stationary at the maximum detectable range on radar bore sight. The UWB transmitter is also assumed to be on radar bore sight yet its range to the radar receiver is varied to induce desired received power variation.

The simulation goal is to determine how the interfering signals impact the radar's ability to detect targets reliably. As modeled, the results presented here represent a worst case analysis of both the GPS M-Code and UWB interferences effects on an air traffic control (ATC) radar. For illustration purposes, the simulation parameters considered are consistent with operational parameters of the Air Route Surveillance Radar Model 4 (ARSR-4) [14] system.

1.5 Thesis Organization

More detailed information on GPS M-Code signal structure, UWB signal structure and radar detection is presented in Chapter 2. Chapter 3 provides the simulation methodology, including the model used and results obtained from simulation and analysis. Finally, a summary of the results and recommendations for future research are presented in Chapter 4.

II. Modern Signal Structure and Radar Theory Background

2.1 Overview

This chapter presents detailed information on the two modern signals considered under this research, namely, the GPS M-Code and impulse-like UWB waveforms. Sufficient radar detection theory is presented to permit understanding of how the modern signals act as interfering sources and degrade detection performance. The focus of the M-Code signal discussion is on signal generation and structure as compared with current GPS course acquisition (C/A) and precision (P) codes. A more thorough discussion of the C/A and P-codes can be found in [5, 15]. While there are many types of UWB waveforms that could be considered, the UWB discussion pertains only to the signal generation and structure of impulse-like UWB waveforms. Specifically, this work considers a biorthogonal pulse position modulated (BPPM) waveform whereby Gaussian monocycles are time shifted in accordance with data modulation. The radar theory discussions focus on pulse characteristics, the range equation, path length attenuation via Friis Transmission equation, target detection, pulse compression and pulse integration.

2.2 GPS M-Code Signal

The M-Code signal was designed with specific upgrade goals, including [10]:

- Better jamming resistance than current P(Y)-coded signals as accomplished through higher transmit power while inducing minimal interference to existing C/A-code or P(Y)-code operation.

- Compatibility with prevention jamming against enemy GPS use.
- More robust signal acquisition.
- Comparable, perhaps better, performance than the P(Y)-code signal.
- Coexistence with current signals operating at both L1 and L2, not interfering with current or future military user equipment.
- Simple and low-risk implementation on both space vehicles and future equipment. (must be as power efficient as possible).

The M-Code was designed having the following characteristics:

- Binary Offset Carrier (BOC) modulated signal using a subcarrier frequency of 10.23 MHz.
- Spreading code rate of 5.115 M spreading bits-per-second.

This combination is denoted BOC(10.23,5.115) and abbreviated BOC(10,5) [6].

The transmitted M-Code signal is mathematically represented by [16]:

$$S_M(t) = \sqrt{2P_M}\, d_M(t) SW(t) PN_5(t) \cos\left(\omega_{L1,2} t + \theta\right) \tag{2.1}$$

where

P_M = Transmitted M-Code power

$d_M(t)$ = M-Code data modulated waveform (25 or 100 bps)

$SW(t)$ = 10.23 MHz Square wave carrier

$PN_5(t)$ = 5.115 MHz Pseudorandom code

$\omega_{L1,2}$ = L1 or L2 angular frequency

θ = Phase

The main desired result of using BOC(10,5) modulation is to have a majority of the power displaced from the carrier frequency (f_c) and concentrated at ±10.23 MHz about f_c as shown in Fig. 2.1 (f_s = 10.23 MHz and f_c = 5.115 MHz) [6]. The M-Code Power Spectral Density (PSD) is given by [4] as

$$PSD_{BOC(f_s,f_c)}(f) = f_c \left(\frac{\sin\left(\frac{\pi f}{2f_s}\right)\sin\left(\frac{\pi f}{f_c}\right)}{\pi f \cos\left(\frac{\pi f}{2f_s}\right)} \right)^2 \tag{2.2}$$

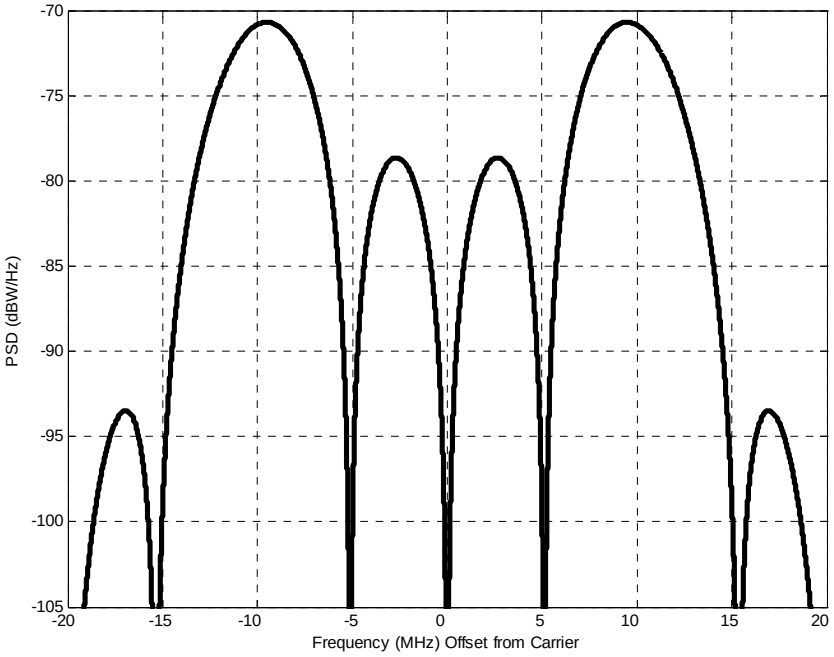

Figure 2.1: PSD of BOC (10,5) M-Code Modulation [6].

One key design goal of M-Code implementation was to receive the M-Code at higher power levels without degrading existing system performance [17]. As seen in Fig. 2.2, the M-Code's peak spectral responses are separated from the current GPS signal responses, though the separation is not an absolute separation. The frequency at which the M-Code signal power peaks is distinctly separate from the C/A and P(Y) code. There is a major overlap of M-Code side lobe responses and the P(Y) response throughout the spectrum [6]. Table 2.1 shows minimum and maximum received RF signal power levels for the M-Code, listed by satellite production version [4].

Table 2.1: Received RF M-Code Signal Strength (dBW) [4]

Production Version	Min	Max
Block IIF	-160	-153
Block IIR-M	-160	-153
Future SVs	-158	-131

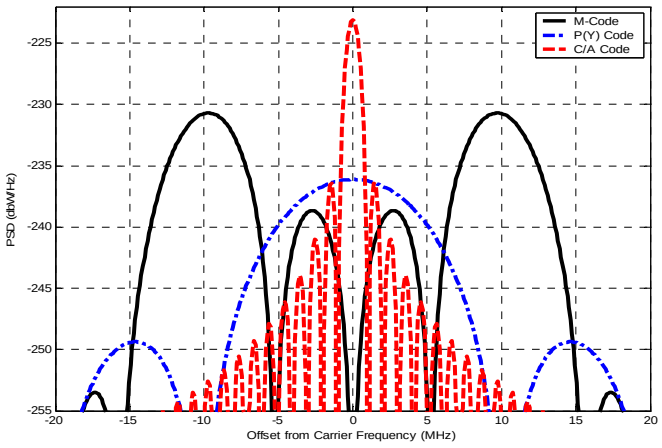

Figure 2.2: PSD Comparison of C/A, P(Y), and M-Code [6].

2.3 Ultra Wide Band (UWB) Signal

For initial UWB performance evaluation, direct sequence time hopped (TH) coding is combined with 4-ary Biorthogonal Pulse Position Modulation (BPPM) [2] to generate the second interferer considered for radar detection analysis. Binary (orthogonal) PPM techniques using UWB waveforms have been successfully employed as well [2] and their effects on radar detection performance (robustness and/or degradation thereof) will serve as a baseline for characterizing interference effects of 4-ary BPPM. The transmitted UWB waveform of this work (accounting for transmit and receive antenna effects) is the second derivative of a Gaussian impulse given by [2],

$$w(t) = \left[1 - 4\pi \left(\frac{t}{\tau_m} \right)^2 \right] \cdot \exp\left[-2\pi \left(\frac{t}{\tau_m} \right)^2 \right] \tag{2.3}$$

where impulse width parameter τ_m is approximately equal to $0.4 \times T_w$, the impulse width. For generating signals in the 5.0 GHz frequency range, pulse durations on the order of $T_w = 0.2$ nsec are used. Bi-orthogonal UWB modulation is achieved by combining binary antipodal signaling with binary Pulse Position Modulation (PPM). The resultant transmitted UWB signal using the fundamental waveform of (2.3) can be analytically represented by

$$s(t) = \sqrt{P_s} \sum_{i=-\infty}^{\infty} (-1)^{a_{2i}} \cdot w\left[t - (-1)^{[a_{2i} \oplus a_{2i-1}]} \cdot \Delta \right] \tag{2.4}$$

where P_s is average power, i is symbol number, a_{2i} and a_{2i-1} are binary input data equaling 1 or 0, $\oplus$ represents Modulo-2 addition, and Δ is the relative PPM offset. For

this work, a PPM relative offset of $\Delta = T_s/4 = T_w/2 = 0.073$ nsec is used, where T_s is the symbol duration. BPPM was chosen for the UWB portion of this work since its power spectral density does not have the spikes that Pulse Position Modulation does. For this reason, it is assumed that modern UWB systems will more likely incorporate BPPM than PPM. Figure 2.3 shows the power spectral densities (PSDs) for equal energy Gaussian monocycle pulse-trains, including one for binary PPM (solid line), one for binary PAM (dashed line), and one for 4-ary bi-orthogonal PPM (dotted) [24]. Figure 2.3 clearly illustrates how 1) the peak PSD response of the PAM and BPPM UWB waveforms is approximately 40 dB below that of PPM, and 2) the PPM "spectral lines" are not present in either the PAM or BPPM cases. Though the PSD results of PAM and BPPM are similar, UWB was selected for use in the work. It is important to note that the Federal Communication Commission (FCC) mandates that all

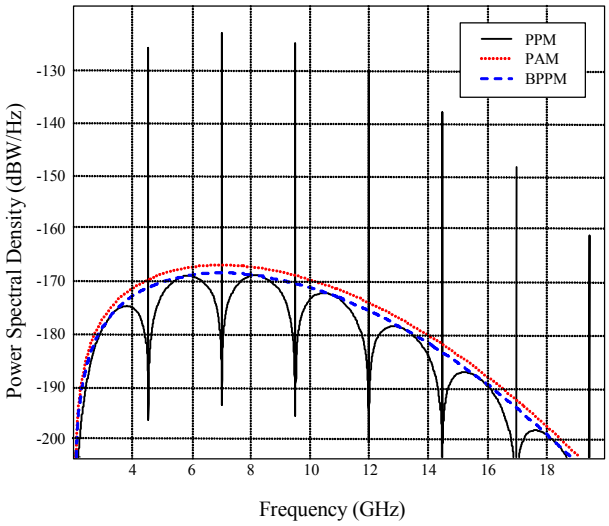

Figure 2.3: PSD Comparison of PPM, PAM and BPPM UWB [24]

unlicensed UWB systems maintain no more than -41.3 dBm effective isotropic radiated power (EIRP) in the 3.1 to 10.6 GHz band, as seen in Fig 2.4 [3] and listed in Table 2.2.

Table 2.2: Hand-Held (Outdoor) FCC UWB Power Specifications

Frequency (MHz)	EIRP (dBm)
960-1610	-75.3
1610-1900	-63.3
1900-3100	-61.3
3100-10600	-41.3
Above 10600	-61.3

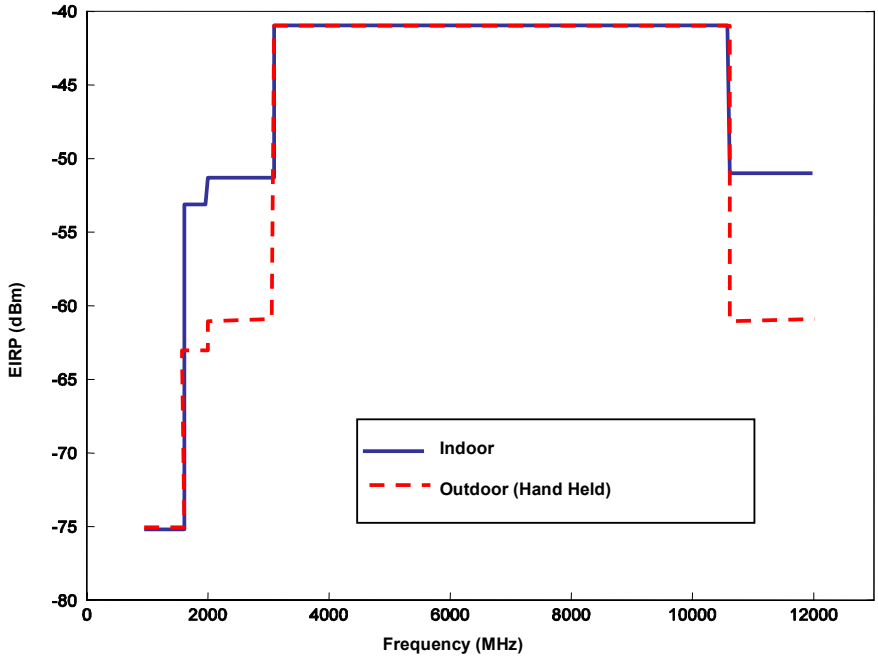

Figure 2.4: FCC Unlicensed UWB Operational EIRP Limitations [2]

For this reason, the PSDs of each of the three waveforms previously mentioned were generated and scaled to ensure they met FCC power limitations.

2.4 Radar Detection Theory

Radars operate by radiating electromagnetic energy and processing the reflected (returned) energy for detection and range determination. Basic radar principles are depicted in Fig. 2.5 as reproduced from [7].

2.4.1 Basic Radar Pulse

Radars transmit a radio wave that propagates through the channel and reaches an object. In most cases, this object reflects a portion of the radio wave energy back toward the radar. To avoid problems with interference, assuming mono-static radar operation whereby the radar shares one antenna between transmit and receive functions, the radio wave energy is transmitted in pulses [6].

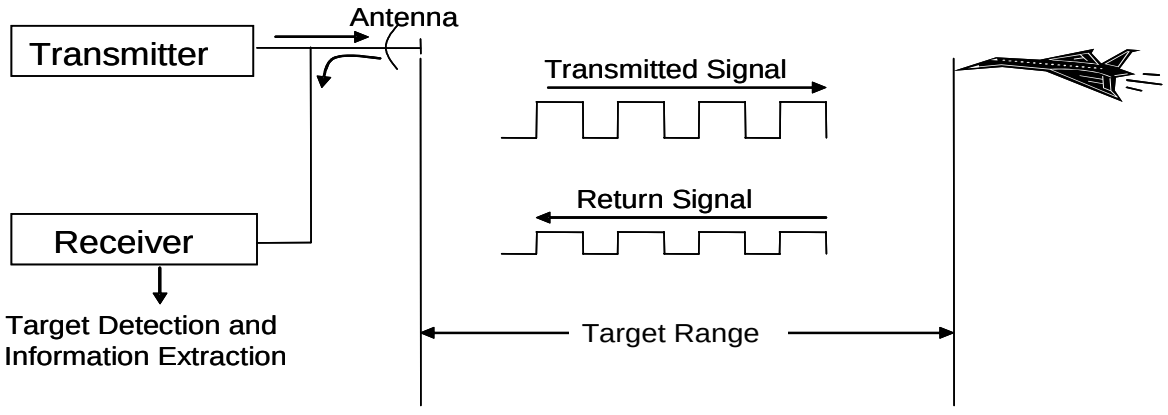

Figure 2.5: Illustration of Basic Radar Principle [7].

The following terms are used to describe radar pulse transmission :

- Pulse Width (τ): Time duration of transmitted pulse
- Interpulse period (T): Time between the leading edges of successive pulse transmissions
- Pulse Repetition Frequency ($f_r = 1/T$): Rate at which pulses are transmitted

During each interpulse period T, the radar transmits energy for τ seconds and then 'listens' for target returns for the remainder of the period. Energy returning from a target located at a distance R from the radar, returns to the radar with a total time delay Δt (two way propagation time) given by:

$$\Delta t = \frac{2 \cdot R}{c} \tag{2.5}$$

where c is the speed of light. Assuming Δt is less than or equal to T, the maximum unambiguous range ($R_{\max}$) can be calculated. When Δt becomes greater than T, an ambiguous range condition occurs, i.e., it is not known which of the transmitted pulses the received energy is associated with [6].

$$R_{\max} = \frac{c \cdot T}{2} = \frac{c}{2 \cdot f_r} \tag{2.6}$$

An example of a range ambiguous situation is shown in Fig. 2.6 as reproduced from the work in [4]. Pulse 1 is transmitted and returns from a target at range $R_1 = (c \cdot \Delta t)/2$, represented by Echo 1. Echo 2 could be a return from the same target and Pulse 2, or it could be a return from a more distant target at range R_2 and Pulse 1; a range ambiguous

situation given that Echo 2 could be interpreted as a return from either Pulse 1 or Pulse 2 [18].

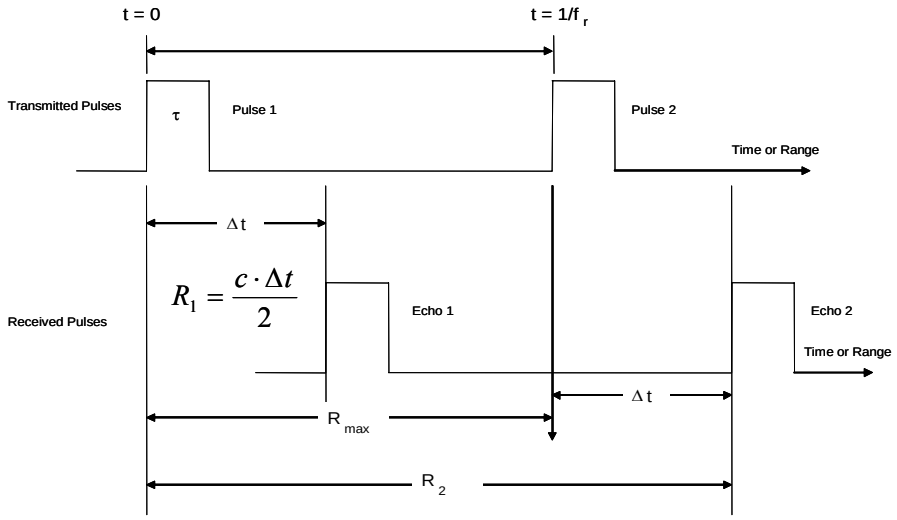

Figure 2.6: Range Ambiguity Illustration [6]

2.4.2 Radar Range Equation

Following the development of [19], the radar equation is derived. Radar detection range is primarily a function of three parameters: 1) transmitted power, 2) antenna gain and 3) receiver sensitivity [7]. If power P is radiated uniformly in all directions from an antenna, the power density at range R from the antenna [6] is

$$PowerDensity = \frac{P}{4\pi R^2} \tag{2.7}$$

This is not the case for most radar systems where a directive (non-uniform) antenna is generally used. The antenna directivity can be accounted for by incorporating antenna gain into (2.7). Antenna gain at a particular angle θ is defined as the ratio of radiation intensity at θ to the radiation intensity of a uniformly radiating antenna [19]. At

$\theta = 0$, the maximum gain G for the antenna is related to its physical area A [6] and is given by

$$G = \frac{4\pi A \rho_a}{\lambda^2} \tag{2.8}$$

where ρ_a is antenna efficiency and λ is the wavelength of the transmitted wave. The radiated power density of a directed antenna (P_{da}) is obtained by modifying (2.7) to include (2.8) as is given by [6]

$$P_{da} = \frac{PG}{4\pi R^2} \tag{2.9}$$

The amount of energy returning to the radar is also dependant on the target's Radar Cross Section (RCS), denoted by σ and measured in units of area. Target RCS is normally determined experimentally [6, 15]. The power received, P_r, at the radar can be calculated as

$$P_r = \frac{P(G\lambda)^2 \sigma}{(4\pi)^3 R^4} \tag{2.10}$$

The target return signal is almost always corrupted by interference and/or noise. The interfering M-Code or UWB signals, which are received by the radar, are examples of noise which potentially impact radar detection performance. Thermal noise, resulting from thermal agitation of electrons in the receiver, is a noise contribution generated at the receiver [6]. Thermal noise power N_T can be represented by

$$N_T = kTB_n \tag{2.11}$$

where k is Boltzmann's constant, $k = 1.38 \times 10^{-23}$ joules/degree Kelvin, T is the noise temperature in degrees Kelvin, and noise bandwidth B_n is expressed in Hz. As stated

earlier, this is only a portion of the total received noise power. The total received noise power is accounted for by multiplying (2.11) by the receiver noise figure [6], F_n

$$N = F_n kTB_n \tag{2.12}$$

The radar equation is then recast [6] using the received power obtained in (2.10), denoted as *S*, and the noise power in (2.12) to represent the signal-to-noise ratio *S/N* as

$$\frac{S}{N} = \frac{P(G\lambda)^2 \sigma}{(4\pi)^3 R^4 F_n kTB_n} \tag{2.13}$$

2.5 Range Equation

In conjunction with determining radar detection characteristics, it is desirable to know how radar detection performance corresponds to the separation between the interfering source and the radar receiver. Since the M-Code case is set up to ensure "returned radar energy is from a stationary airborne point target located at the maximum required detection range," separation distance is fixed. However, in the UWB case, transmit power is fixed and the separation distance varies according to the level of interfering power necessary at the radar receiver to degrade detection performance. The Friis transmission equation [25], as given by (2.14), is used to calculate separation,

$$P_r = P_t \cdot G_t(\theta_r, \phi_r) \cdot G_r(\theta_t, \phi_t) \cdot \left(\frac{PLF}{L_{FS}} \right) \tag{2.14}$$

where *PLF* is polarization loss factor, P_r is *received* antenna output power (Watts), P_t is *transmit* antenna input power (Watts), $G(\theta, \phi)$ is gain in the θ / ϕ direction (Unitless) and L_{FS} is free-space path loss (Unitless). Free-space path loss L_{FS} can be derived using (2.15) and is a function of frequency *f*, propagation distance *R (R* is the separation

distance between transmitter and receiver in meters), and the speed-of-light ($c \approx 3.0\text{x}10^8$ meters/second) [25].

$$L_{FS} = \left(\frac{4 \cdot \pi \cdot f \cdot R}{c} \right)^2 \tag{2.15}$$

2.6 Radar Target Detection

Simulation results presented here are obtained using a correlator implementation of a matched filter where the radar receiver processes the returned signal plus added noise. A block diagram of the radar matched filter detection process is shown in Fig. 2.7.

In the detection process of Fig. 2.7, the received signal is bandpass filtered prior to matched filtering. For matched filtering, the bandpass filtered signal is correlated with a replica of the originally transmitted radar signal, or reference signal. This correlation results in a correlator output value which represents a measure of the consistency between received signal and the reference signal. Next, the threshold stage compares the correlator output to a predetermined value, or threshold. When the output exceeds the threshold, a target is declared present. It is possible for a target to be declared present when no target return is actually present, i.e. only noise is present. This condition results

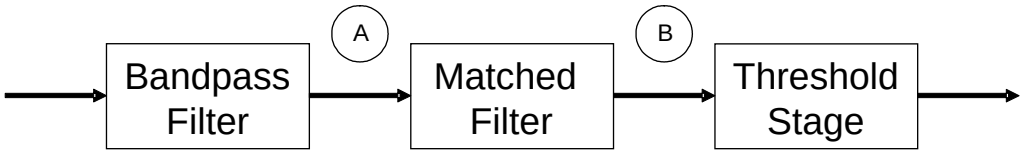

Figure 2.7: Radar Matched Filter Detection Process [6]

in what is called a *false alarm*. It is also possible for a target return to actually be present and go undeclared, i.e. the correlator output falls below the threshold when a target return plus noise is present. This condition is known as a *missed detection* and yields a Probability of Detection (P_D) less than one. If the threshold is lowered, the missed target can be detected at the expense of increasing the Probability of False Alarm (P_{FA}). One way to increase P_D without increasing P_{FA} is to increase the returned signal strength, thereby increasing the effective signal-to-noise ratio (SNR) [6].

2.7 Radar Pulse Compression

It is generally desirable to receive a large amount of return target energy over large distances, but still achieve the same range resolution as is obtainable with a short pulse duration. One way to obtain this desired outcome is by introducing pulse compression. Pulse compression can be accomplished using frequency and/or phase modulation to expand the signal bandwidth. Pulse compression is used to achieve the benefits of a short pulse radar system, i.e. range resolution, range accuracy, minimum detection range, etc, while keeping within the constraints of peak power limitations imposed by practical transmitters. Though there are many ways for obtaining pulse compression, the two common methods considered here are linear frequency modulation (LFM) and biphase coding [6].

2.7.1 LFM Pulse Compression.

In LFM pulse compression the transmitter uses a frequency modulated signal with the signal's frequency either increasing (up-chirp) or decreasing (down-chirp) linearly from a initial to final frequency value. The receiver contains a pulse compression filter (effectively a matched filter). When the LFM echo passes through the pulse compression filter it effectively speeds up the higher frequencies relative to the lower frequencies to compress the pulse to a width of $1/B$, where B is the difference between the higher and lower frequency limits. Thus, the pulse bandwidth is successfully expanded while enabling the pulse to perform with the benefits of a short pulse radar system [6].

2.7.2 Phase Coded Pulse Compression.

In phase coded pulse compression, the original pulse duration τ is divided into N equal width intervals, or chips, of duration τ_c. This division effectively increases the pulse bandwidth by a factor of $1/\tau_c$. The phase of each sub-pulse is chosen to be either 0 or π radians (bi-phase modulation). The phase value choice for each sub-pulse may be random, with some 'random' selections being better for specific radar applications. One 'good' selection of phase values is one in which the phase-coded waveform has equal time-side lobes. The binary phase-coded sequences that provide such results are called Barker codes. The thirteen known Barker codes are shown in Table 2.3 below.

Examples of an uncompressed sinusoidal pulse, an LFM sinusoid (up chirp) and a Barker coded (length 13) sinusoid (all equal duration) are shown in Fig. 2.8. The

corresponding spectral response of each of the three signal types, normalized by the magnitude of the sinusoid, is shown in Fig 2.9 [6].

Table 2.3: Known Barker Codes [21]

Code Length	Code Elements
2	+- , ++
3	++-
4	++-+ , +++-
5	+++-+
7	+++--+-
11	+++---+--+-
13	+++++--++-+-+

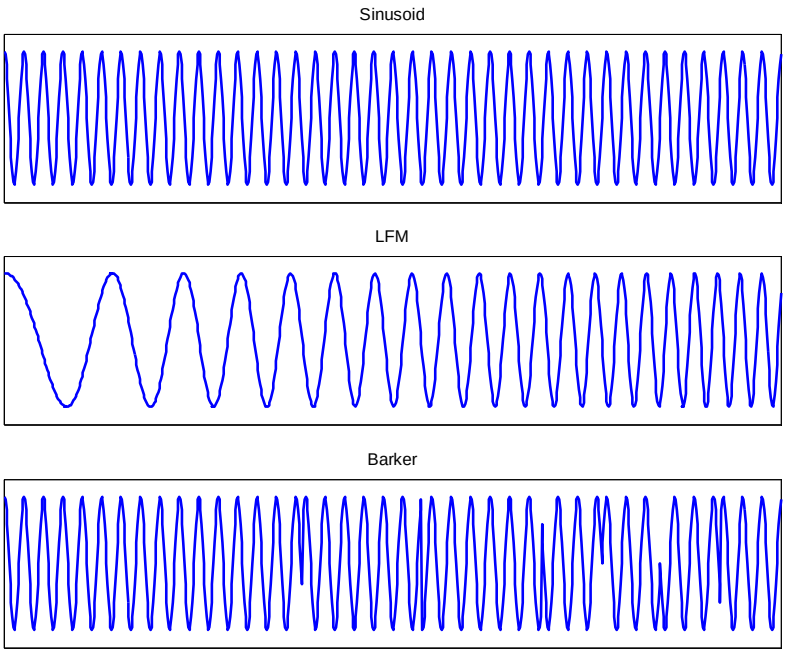

Figure 2.8: Time Response of Sinusoidal Pulse (top), an LFM Sinusoid (middle) and a Barker Coded Sinusoid (bottom) [6]

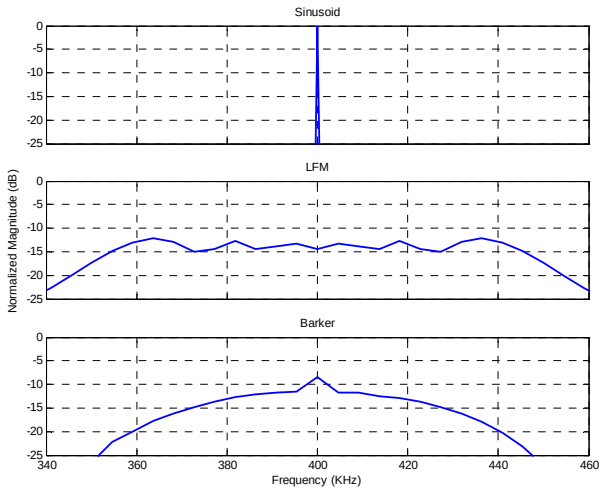

Figure 2.9: Normalized Spectral Response of Sinusoidal Pulse (top), LFM Sinusoid (middle) and Barker Coded Sinusoid (bottom) [6]

2.8 Radar Pulse Integration

One way to significantly improve P_D is to use a technique termed *pulse integration*. Prior to the detection process, multiple pulse responses can be combined from a particular target during each radar scan [21] to improve effective signal to noise ratio. To gain benefits afforded by the integration process, returned pulses (or pulse responses) can be summed together either prior to or after detection. If integration occurs *prior* to detection, the system is deemed as using pre-detection, or *coherent integration*. If integration occurs *after* detection, the system is deemed as using post-detection, or *noncoherent integration.* In coherent integration, the phase information of the target return must be kept intact for the process to be effective. This action is not necessary for noncoherent integration, since the phase information is altered by the detection process. The following signal-to-noise ratio (SNR) relationship applies for ideal coherent pulse integration [21]

$$SNR_{Post} = nSNR_{\Pr e} \tag{2.16}$$

where n is the number of pulses integrated, SNR_{Post} is the SNR after coherent integration, and SNR_{Pre} is single pulse SNR before coherent integration; note that (2.16) assumes the single pulse SNR is identical for all pulses integrated. If the same number of pulses n were used with non-coherent integration, the expected SNR improvement would be less than n. Even though the benefits afforded by noncoherent integration are not as great as those of coherent integration, noncoherent integration can be beneficial given that it is usually easier to implement [6].

2.9 Summary

This chapter presented analytical expressions for the modern signals considered under the research, namely, the proposed GPS M-Code signal and a time modulated impulse-like UWB waveform. A short discussion of radar theory was also presented, including a derivation of the radar equation, separation and propagation path loss analysis, the detection process, pulse compression and pulse integration. This information provides the theoretical and conceptual basis used for the simulation methodology, results and analysis presented in the following chapters.

III. Simulation Methodology, Results and Analysis

3.1 Overview

This chapter presents the simulation methodology and results of both the M-Code and the UWB interference effects on Probability of Detection (P_D). The simulation was developed to permit characterizing M-Code and UWB signal effects on radar system detection capability. M-Code simulation results of [6] were regenerated and used to provide initial verification and validation of the model introduced here. Given successful model validation using the M-Code interference, the UWB interferer was introduced and new detection results generated.

Presentation of the simulation methodology and results is divided into three parts. First, the radar model is introduced as used for both interfering cases and some general groundwork provided. Second, the specific methodology and results pertaining to M-Code analysis is presented. Finally, the specific methodology and results pertaining to UWB analysis is presented.

Analysis of interferer effects on radar detection performance is segmented into four categories: 1) baseline performance (no interference present), 2) introduction of interference, 3) introduction of pulse compression, and 4) introduction of pulse integration. Interference gating (periodic sampling of the interference during pulse arrival at intervals equaling the radar PRF) is introduced and applied to all results shown in this work. Furthermore, after baseline performance characterization, signal and noise powers are set to achieve a specific P_D such that interference effects are isolated/identifiable for each scenario considered. When pulse integration is introduced,

new baseline results are generated with subsequent results once again being obtained with fixed signal and noise powers. Both LFM and Barker coding are introduced into the radar to provide pulse compression given such techniques are commonly used to enhance radar range resolution capability.

3.2 Simulation Description (Overall)

This section lays the groundwork for the simulating the effects of interference on radar detection performance. Simulation parameters, radar model, Albersheim's relationship and the process of adding interference are all concepts explained in this section.

3.2.1 Radar Simulation Parameters (ARSR-4)

For computational and illustrative purposes, operational parameters of the ARSR-4 (air route surveillance radar) are used for the basic radar simulation. The following pertinent information is taken from *Instruction Book, Field Maintenance, ARSR-4 System, Type FA-10331 Sections 1-10* [14].

The ARSR-4 is used jointly by the Federal Aviation Administration (FAA) and the United States Air Force (USAF) for three-dimensional (3D), long range radar detection. The system provides 360 degrees azimuth coverage at ranges up to 250 nautical miles, altitudes up to 100,000 feet, and for elevation angles of -7 to +30 degrees.

The ARSR-4 radar is designed to detect very small targets ($\sigma = 0.1$ m^2) at ranges up to 92 nmi and larger targets ($\sigma = 2.2$ m^2) out to 200 nmi. The minimum range requirement is 5 nmi with range resolution of 1/16 nmi. A relatively long pulse width (150 μsecs) is used to achieve these requirements. The wide pulse is made up of two

sub-pulses (60 and 90 μsecs) transmitted at two different frequencies that are separated by 82.8572 MHz; the 90 μsec pulse is used at the lower frequency to meet detection requirements and the 60 μsec pulse is used at the higher frequency to meet the 5 nmi range requirement. The 90 μsec pulse is transmitted first followed by the 60 μsec pulse. Following transmission of the 60 μsec pulse, the radar receiver turns on to begin processing radar echoes. Operating parameters for the ARSR-4 are summarized in Table 3.1.

Table 3.1: Operating Parameters for the ARSR-4 System [14]

Parameter	Value
Peak Transmit Power	63.765 kW
Average Power	2.55 kW
Waveform Duty Cycle	4.32 %
Antenna Transmit Gain	37.7 dB
Antenna Receive Gain	40.91 dB (Max)
Frequency Range	1215-1400 MHz (Diplex)
Pulse Repetition Freq (PRF)	288 Hz
Scan Time	12 Secs
Azimuth Beamwidth	1.4 Degrees
Pulses Integration	8 Pulses

.

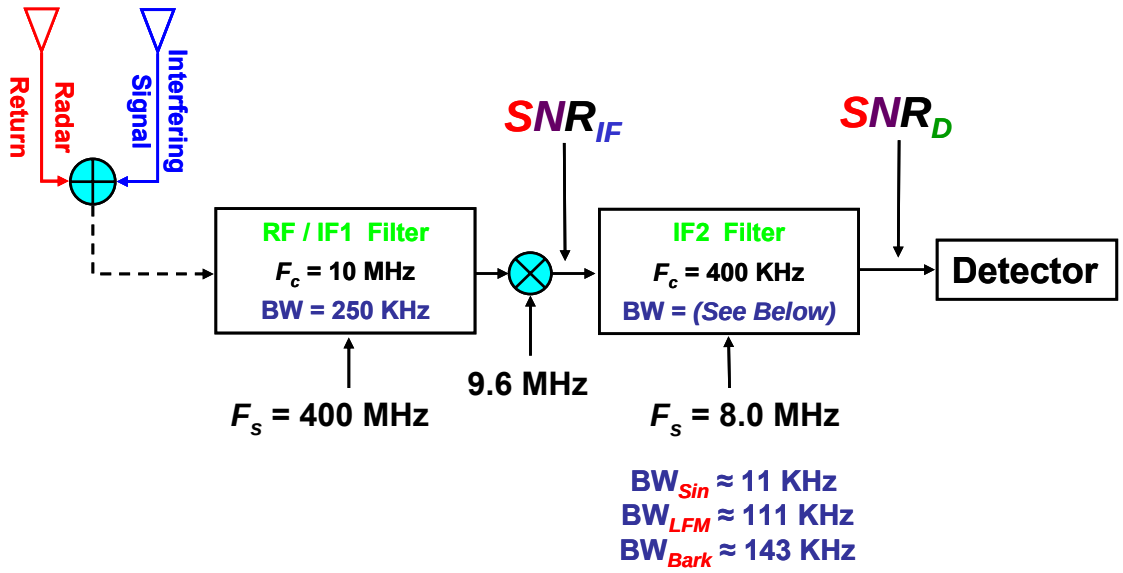

Figure 3.1: Simulation Radar Model

3.2.2 Simulated Radar Model

The basic radar model used for simulations is shown in Fig. 3.1 above. Exact details of various model components and implementation thereof will be explained on a phase-by-phase basis. For baseline cases, the only inputs to the system are the radar return (sinusoidal pulse), *s(t)*, and the thermal noise term, *n(t)*.

Initially, the radar return signal *s(t)* is a pulsed sinusoid of duration $\tau = 90$ μsec and centered at an IF frequency of 400 KHz. Although not illustrated in Fig. 3.1, thermal noise *n(t)* is modeled as zero-mean *AWGN* and is assumed present with the received radar pulse and eventually, the interfering signal. The *SNR* into the IF filter is denoted as SNR_{IF} and is determined by taking the ratio of average signal power (P_s) to average noise

power (P_n) at the IF filter input, where the average power of the sampled signal and noise waveforms [6] can be approximated as

$$P_s \approx \frac{1}{N}\sum_{j=1}^{N} s^2(t_j) \tag{3.1}$$

$$P_n \approx \frac{1}{N}\sum_{j=1}^{N} n^2(t_j) \tag{3.2}$$

In (3.1) and (3.2) N is the number of samples in a given duration and a normalized 1Ω load is assumed. In addition, in determining the average noise power, a noise bandwidth of $1/\Delta t$ is implied where Δt is the sample time. For simulations in this work, $\Delta t = 1.25\times10^{-7}$ secs, at the IF filter, yielding a simulated IF input noise bandwidth of 8.0 MHz [6].

Since the radar return signal is filtered at both levels in practical systems, the radar model is designed to incorporate return signal filtering at both the RF and IF levels. The RF/IF1 filter bandwidth is fixed at 250 KHz which is sufficient to pass nearly 100% of the signal energy for all radar waveforms considered (using fixed $\tau = 90$ μsec for the unmodulated sinusoid, LFM and Barker coded waveforms). Per Fig. 3.1, the interfering signals and radar return pass through both the RF/IF1 filter and IF2 filters.

The IF2 filter bandwidth for simulations without pulse compression is set to 1/90 μsecs, or approximately 11.0 KHz, which represents the approximate bandwidth measured between the -4.0 dB power points. Bandwidths on the order of $1/\tau$ are typical for receivers of this type [6].

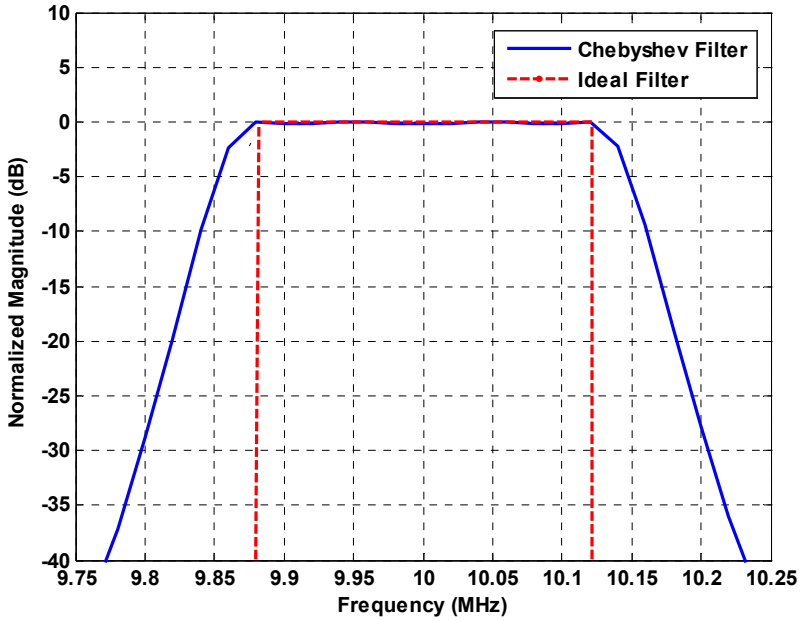

Figure 3.2: Filter Response of an Ideal Filter and a 4th-Order Chebyshev Filter

For both the RF/IF1 and IF2 filters, a 4th-order Chebyshev bandpass filter having 10^{-7} dB bandpass ripple was employed. The ideal bandpass filter response and simulated Chebyshev filter response for a 250 KHz filter centered at 10 MHz is shown in Fig. 3.2 above. The IF2 filtering operation yields both filtered signal and noise components that are input to the detector. The *SNR* at the detector input is denoted SNR_D and is determined in the same manner used to determine SNR_{IF}, except the signal and noise powers are approximated at the IF2 output.

A matched filter detector (correlator implementation) is used to 'match' the filtered received signal (generally the radar return plus noise plus interference) with a replica of transmitted signal *s(t)* (correlator reference signal). The matched

filter/correlator output, or test statistic $z_{tot}(t)$, is then compared to a predetermined threshold $z_T(t)$ to determine target presence. Whenever $z_{tot}(t)$ exceeds $z_T(t)$, target presence is declared. If $z_{tot}(t)$ falls below $z_T(t)$ no target is declared. Given $n(t)$ is always assumed present, it impacts the detector process by contributing a noise component $z_n(t)$ to the total correlator output $z_{tot}(t)$. Likewise, for cases when interference is introduced the detection process is further impacted by an interfering component $z_{int}(t)$. Thus, the total test statistic becomes $z_{tot}(t) = z_{sig}(t) + z_n(t) + z_{int}(t)$ which is compared with threshold $z_T(t)$ for making detection decisions. For baseline simulations with *no interference present*, threshold $z_T(t)$ is established to achieve a constant P_{FA} (CFAR) with *only noise* present at the matched filter input, i.e., $z_{tot}(t) = z_n(t)$ is used to set the threshold. For all simulations with *interference present*, threshold $z_T(t)$ is established to achieve a constant P_{FA} (CFAR) with *both noise and interference* present at the matched filter input, i.e., $z_{tot}(t) = z_n(t) + z_{int}(t)$ is used to set the threshold. For each random realization of noise and/or interference (as appropriate) input to the receiver, $z_{tot}(t)$ is generated and stored.

After a sufficient number of total test statistic values are collected, they are sorted and a threshold value assigned based on the $N_{real} - (P_{FA} \times N_{real})$ largest $z_{tot}(t)$ values, where N_{real} is the number of realizations required to reliably simulate the desired P_{FA}. A common rule-of-thumb for radar detection simulations is that the number of required realizations $N_{real} = 10/P_{FA}$ [15]. Thus, for all simulations in this work using a fixed $P_{FA} = 0.01$, $N_{real} = 1000$ noise realizations are used with threshold $z_T(t)$ set equal to the 990^{th} largest $z_{tot}(t)$ value as illustrated in Fig. 3.3 [6].

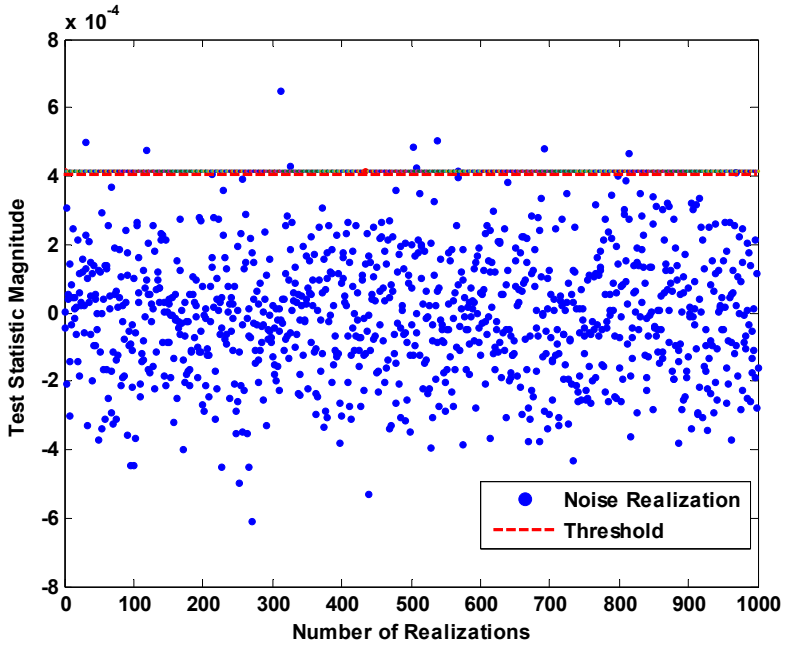

Figure 3.3: Threshold Level Illustration Using 1000 Noise Realizations

After threshold setting, the matched filtering/detection process is repeated with the target return signal added to each noise realization and a new test statistic is produced as $z_{tot}(t) = z_{sig}(t) + z_n(t)$. Probability of detection (P_D) is then determined by 1) taking the total number of $z_{tot}(t)$ values exceeding $z_T(t)$, and then 2) dividing this number by the total number of realizations ($N_{real} = 1000$ in this case). This P_D is valid for a given P_{FA} and SNR_D. To generate a complete P_D versus SNR_D curve for given P_{FA}, this process is repeated over the range of desired SNR_D values where SNR_D is varied by varying the noise power given target return power is fixed.

Due to computational resource limitations and time constraints, the typical P_{FA} values on the order of 10^{-5} were not considered. Rather, a value of $P_{FA} = 10^{-2}$ is used and permits reliable trend analysis as various system powers are changed, e.g., variation in interfering M-Code or UWB signal power.

Figure 3.4 shows representative detection curves for the baseline simulation (no interfering signal present). The radar return signal used to generate the curve is a single pulsed sinusoid of duration of $\tau = 90$ μsecs centered at an IF frequency of 400 kHz (these parameters are consistent with ARSR-4 specifications) [14]. Noise is generated as zero-mean, *AWGN*, with a unit magnitude average power. The value of SNR_D is changed by varying the noise power while keeping the received signal power constant. The simulated P_D curves (solid lines) in Fig. 3.4 were generated by passing the sampled return signal and noise through the IF2 filter. The matched filter detection process was carried out using a CFAR detection threshold for $P_{FA} = 0.01$ (10^{-2}) and $P_{FA} = 0.001$ (10^{-3}) with P_D estimated per the process described above. Albersheim results are discussed in Section 3.2.3.

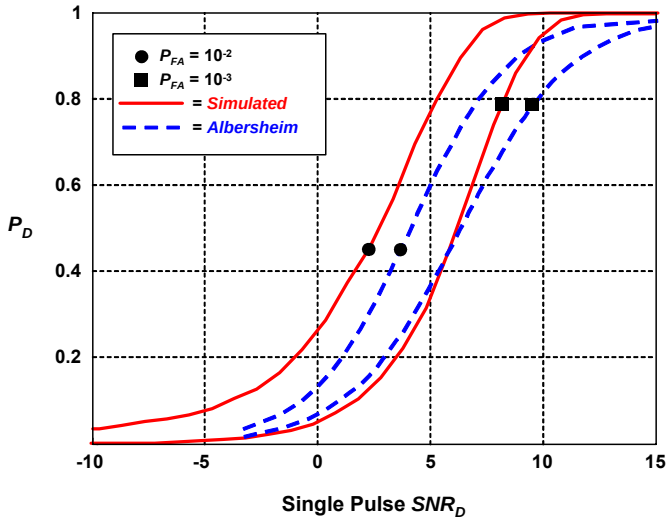

Figure 3.4: Baseline P_D Curves for $P_{FA} = 10^{-2}$ and $P_{FA} = 10^{-3}$

3.2.3 Albersheim's Relationship

In support of validating the radar model of Fig. 3.1 and showing consistency of results presented in Fig. 3.4, the work of Albersheim is introduced. Albersheim developed a simple empirical equation for the relationship between *SNR* (at the detector input), P_D and P_{FA} for single pulse detection [21] and is given as follows:

$$SNR = A + 0.12 \cdot A \cdot B + 1.7 \cdot B \tag{3.3}$$

where $A = ln\,[0.62 / P_{FA}]$ and $B = ln\,[P_D / (1\text{-}P_D)]$.

As presented in (3.3), the *SNR* is given in ratio form versus dB. Although not specified, it is assumed that the *SNR* given by (3.3) is measured at the input to the radar's detector. In the form given by (3.3), Albersheim's expression is said to be accurate to within 0.2 dB for P_{FA} between 10^{-3} and 10^{-7} and P_D between 0.1 and 0.9 for an AWGN channel. Thus, the results presented in Fig. 3.4 are *not directly comparable* given the

simulated results are for "colored" noise resulting from IF2 filtering prior to the detection process. However, they do lend a certain level of credibility to the simulated results given the trends in the simulated curves are consistent with Albersheim's results, especially in the $P_{FA} = 10^{-3}$ case where Albersheim's expression is deemed valid. Factoring in knowledge that Albersheim's relationship is empirically based, and the difference between an AWGN assumption and colored noise implementation, it is assumed here that the radar model of Fig. 3.1 is valid and simulation thereof produces results which are *consistent* with those expected by the radar community.

3.2.4 Addition of Interference Effects

Given baseline performance (with no interference present) results are reliably consistent with expectations, the focus now shifts to adding interference and characterizing the effects thereof on detection performance. The effects of M-Code interference are analyzed first, to include interference gating, pulse compression and finally, pulse integration. Next, the effects of UWB interference are analyzed in a manner paralleling that of the M-Code analysis.

3.3 M-Code Interference Analysis

Before introducing simulation results, it is advantageous to define simulation assumptions and parameters. One important aspect of the M-Code simulations is that they are designed to represent a worst case scenario from the radar receiver perspective, i.e., a scenario causing maximum detection performance degradation. In this case, the M-Code simulation geometry of Fig. 3.5 was used and is summarized as follows [6, 7]:

1. *Returned radar energy is from a stationary airborne point target located at the maximum required detection range.* Thus, maximum propagation path loss occurs, there is no Doppler shift and the return signal is received at minimum detectable power levels.

2. *Initial simulated radar processing is for single pulse detection.* These results represent baseline performance and do not include benefits of pulse compression (range resolution enhancement) or pulse integration (processing gain). Pulse compression and integration are subsequently addressed.

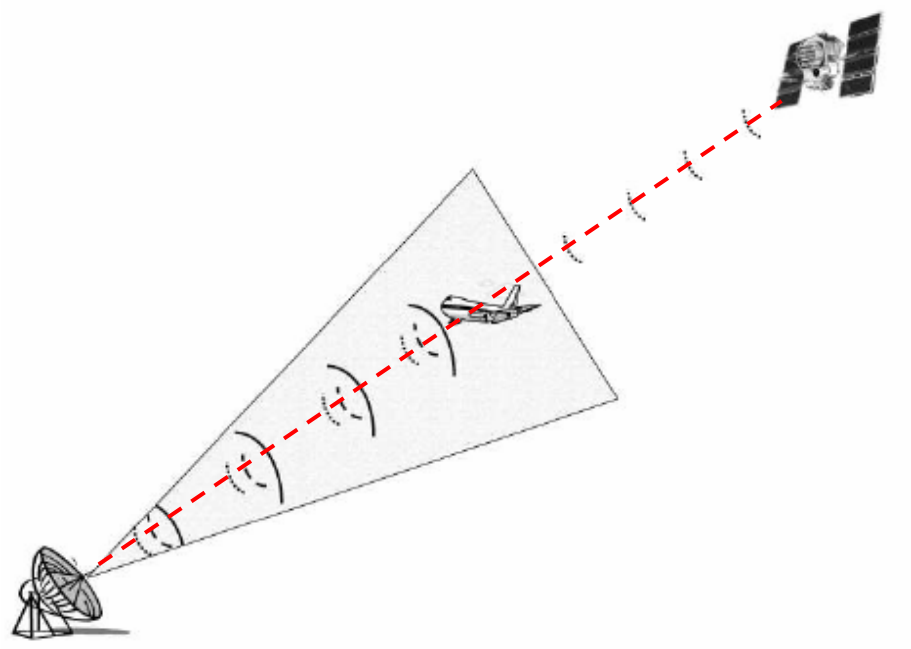

Figure 3.5: M-Code Simulation Geometry [7]

3. *The interfering M-Code signal is received along the same line-of-sight as the target return signal.* The target return and interfering signal experience identical (maximum) antenna gain upon reception.

4. *The radar carrier frequency and peak spectral responses of interfering M-Code signals are coincident.* Thus, maximum received interfering signal power is processed.

5. *The propagation channel is additive white Gaussian noise (AWGN).*

6. *Interfering M-Code signals are continuously received during threshold determination.* The receiver threshold is set to ensure a constant false alarm rate (CFAR) is maintained while both interfering signals and AWGN are present.

7. *The radar receiver bandwidths (RF and IF) are matched to the radar signal under consideration.* The bandwidths are established as the -4.0 dB bandwidth of the radar signal. Waveforms considered include an unmodulated sinusoid, LFM and Barker phase coded pulses, all of which are narrowband relative to interfering signals considered.

With the baseline P_D versus SNR_D results (for a single pulse sinusoidal) in place and simulation assumptions clarified, a P_D level is selected, SNR_D is fixed (fixing average signal and noise power into the detector), and the M-Code signal is added at the receiver input. Figure 3.6 depicts the process of selecting P_D and fixing SNR_D before the interferer is added.

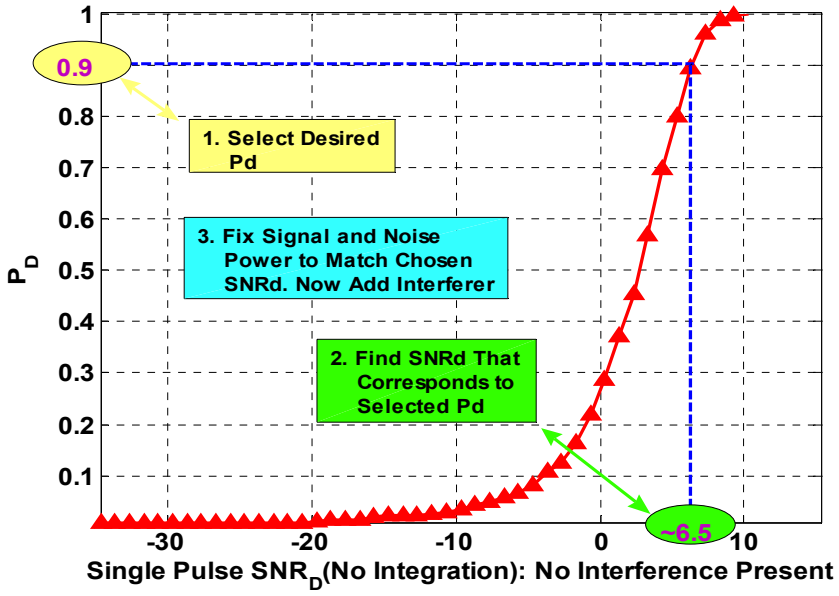

Figure 3.6: P_D and SNR_D Selection Process for Adding Interference

With the M-Code signal present, the return signal power is held constant (at the minimum received power level for a target at the maximum required detection range) and the noise power adjusted to obtain the desired SNR_D value (or equivalently, the desired P_D). This procedure ensures the relative power levels between the radar return signal and the M-Code signal are accurately modeled. The power relationship is maintained by calculating the radar return signal power and the interfering signal power at the receive antenna.

The radar return power at the antenna output was calculated using (2.10) and parameters listed in Table 3.1; including a carrier frequency of 1217.37 MHz, a radar cross section (RCS) of $\sigma = 2.2\text{m}^2$ and a detection range of 200 nmi. The target RCS value and the detection range are consistent with the ARSR-4 system operation [14].

Since the worst case scenario is being simulated, the maximum detection range of 200 nmi was selected (minimum return signal power for a target at this distance). It is reasonably assumed that the M-Code signal has the most interfering effect when the target return signal power is at its minimum. Thus, the received signal power at the receive antenna output is calculated from (2.10) as follows [6, 7]

$$P_r = \frac{\left(63.765\times10^{3}W\right)\left[\left(10^{\frac{37.7}{10}}\right)\left(10^{\frac{40.91}{10}}\right)\left(\frac{\left(3\times10^{8}m/s\right)}{\left(1217.37\times10^{6}Hz\right)}\right)\right]^{2}\left(2.2\ m^{2}\right)}{(4\pi)^{3}(200\ nmi\cdot1852\ m/1.0\ nmi)^{4}} \tag{3.4}$$

$$P_r = 16.56\times10^{-15}W(\approx -138\ dBW)$$

where G = $(10^{37.7/10})$*$(10^{40.91/10})$ since it accounts for the gain of both the transmit and the receive antennas.

Given target return power P_r is fixed under assumptions imposed by this work, the simulated noise power is adjusted to provide the desired SNR_D. For each SNR_D value and calculated P_r, the filtered noise samples are scaled by a gain factor [6] of

$$Gain\ Factor = \sqrt{\frac{P_r}{10^{SNR_D/10}}} \tag{3.5}$$

Since the noise power changes for every desired SNR_D value, a new detection threshold value is required to maintain a constant P_{FA}. The process described previously for determining the threshold value is used repeatedly for each SNR_D value. At this point,

the interfering received power is varied to characterize how the interferer affects the established P_D [6].

The M-Code signal is generated using (2.1) assuming the M-Code PN sequence is random as stated previously. The goal is to effectively simulate a filtered $1/\tau$ (approximately 11.0 KHz) bandwidth portion of the GPS M-Code signal where both the interfering signal peak and the filter are centered at IF2 of 400 KHz. However, since the null-null bandwidth of each the M-Code lobe (approximately 10.0 MHz each) is much greater than the 400 KHz center frequency of the IF2, the pre-filtering step of IF1 and subsequent down-conversion process were implemented to simulate radar receiver front-end processing.

The following process for generating the filtered interfering M-Code signal is based on work in [7]. For the M-Code signal, the down-converted M-Code signal is first generated at a center frequency of 20.23 MHz which places the center of the lower M-Code lobe at approximately 10.0 MHz. The resultant signal is passed through the IF1 filter in Fig. 3.1 which is centered at 10.0 MHz and has a bandwidth of 250 KHz. This bandwidth is wide enough to capture interfering M-Code energy about the peak of the lower main lobe. Finally, the IF1 filtered M-Code signal is down-converted to the 400 KHz center frequency of the IF2 filter. It is assumed that this pre-filtering and down-conversion process is similar to what commonly occurs in radar front-end processing. Once the M-Code signal is passed through the IF2 filter, it has the desired $1/\tau$ bandwidth of approximately 11.0 KHz.

As shown in Fig 3.1, the M-Code signal is added to the return pulse signal at the receive antenna input. The composite received waveform experiences received antenna gain prior to IF1 filtering, down-conversion, IF2 filtering and subsequent matched filter detection. Using the proposed M-Code power levels given in Table 2.1, the M-Code signal was generated having received power levels (incident on the radar antenna) ranging from -160 dBW to -131 dBW.

3.3.1 M-Code Interference Gating

Before proceeding with simulation results having the M-Code present, it is important to understand how the interfering signals are effectively gated (sampled during pulse width τ at intervals dictated by the radar PRF). Work in [6] demonstrated how appropriate interference generation and gating must be incorporated to accurately account for waveform randomness occurring from gate-to-gate. When the composite received waveform is initially sampled (with the first sample occurring at the leading edge of the

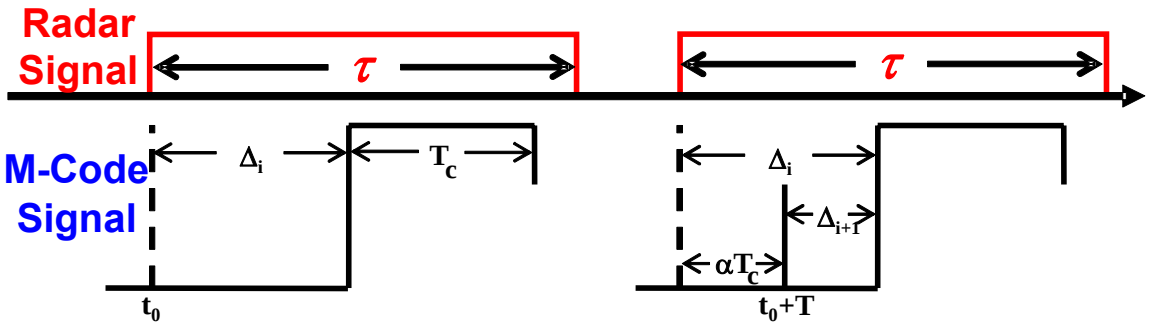

Figure 3.7: Representation of Start Time of Sampled Periodic Waveform with Δ_i greater than or equal to αT_c [6]

first radar pulse) it is sampled at a specific time, say t_o. The time duration from t_o to the next possible transition in the binary waveform can be represented as Δ_i, as shown in Fig. 3.7 above.

During radar interpulse period T, there exists an integer number of chip intervals, kT_c, and some non-integer portion on an interval, αT_c, as expressed in (3.6).

$$T = kT_c + \alpha T_c \tag{3.6}$$

Each time the radar receiver is gated on for pulse duration τ, the periodic M-Code waveform will be sampled at a different starting time depending on the magnitude of the original Δ_i. If as shown in Fig. 3.7, Δ_i is greater than or equal to αT_c, the start time of periodic waveform Δ_{i+1} when the next pulse duration begins is given by

$$\Delta_{i+1} = \Delta_i - \alpha T_c \tag{3.7}$$

However, if Δ_i is less than αT_c as shown in Fig. 3.8, the start time of the periodic waveform Δ_{i+1} when the next pulse duration begins is given by

$$\Delta_{i+1} = \Delta_i + T_c(1-\alpha) \tag{3.8}$$

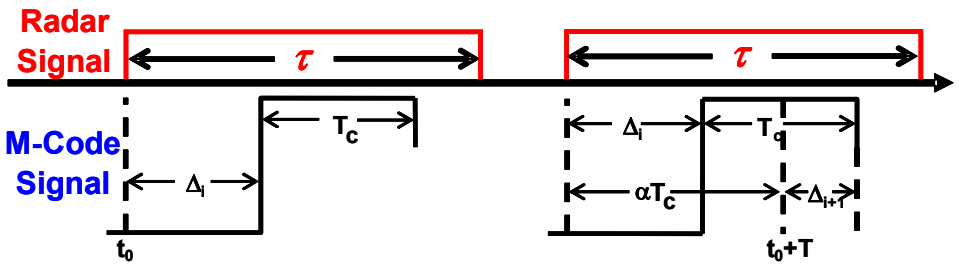

Figure 3.8: Representation of Start Time of Sampled Periodic Waveform with Δ_i less than αT_c [6]

These gating effects were implemented in the simulations such that with each successive radar pulse, starting with the first having Δ_i, the waveform was sampled at the corresponding start time, i.e. Δ_{i+1}, Δ_{i+2}, …, Δ_{i+n}, on each successive pulse [6].

The simulation was run with the gating process and the same parameters given in Table 3.2, and the radar gating process simulated using the starting time synchronization as explained earlier. Though not shown here, the results from [6] indicate a significant detection improvement from non-pulse gating to pulse gating, i.e., greater than 10 dB gain at mid-range of the M-Code power levels (approximately -145 dBW).

The final step was to simulate the interfering GPS signal incorporating the pulse-gating where the simulation parameters were set to actual GPS signal parameters as given in Table 3.2 below.

Since GPS satellites transmit 24 hours a day, 7 days a week, it is reasonable to assume that when the radar sets the threshold the M-Code signal will be present as an

interferer. Thus, for a M-Code interference simulations the M-Code signal is assumed present during threshold determination [6].

Table 3.2: Parameters for Testing Gating Process [6]

	GPS Parameters	Parameters for $\alpha = 0$
Chipping Time (T_c)	5.115 MHz	5.76 MHz
Data Rate	100 bps	288 bps
M-Code IF Signal	20.23 MHz	23.04 MHz
Square-Wave Frequency	10.23 MHz	11.52 MHz

3.3.2 M-Code Interference Effects

The next step was to consider the effects of having the interference present during threshold determination. To analyze the effects, a baseline SNR_D curve for the radar system with no interference present was first generated as shown in Fig. 3.9. Using a constant SNR_D to achieve a specific P_D, the M-Code interference was then introduced into the system and its effects characterized relative to baseline P_D performance. The M-Code signal power was varied from -160 to -131 dBW (minimum to maximum RF signal power levels from Table 2.1) and P_D estimated as before except now the interfering signal was present during threshold determination. Figure 3.6 depicts the process used for selecting a P_D from the baseline plot and choosing the appropriate SNR_D value. The signal and noise powers are then fixed at to achieve this SNR_D and the interference power varied to characterize degradation performance.

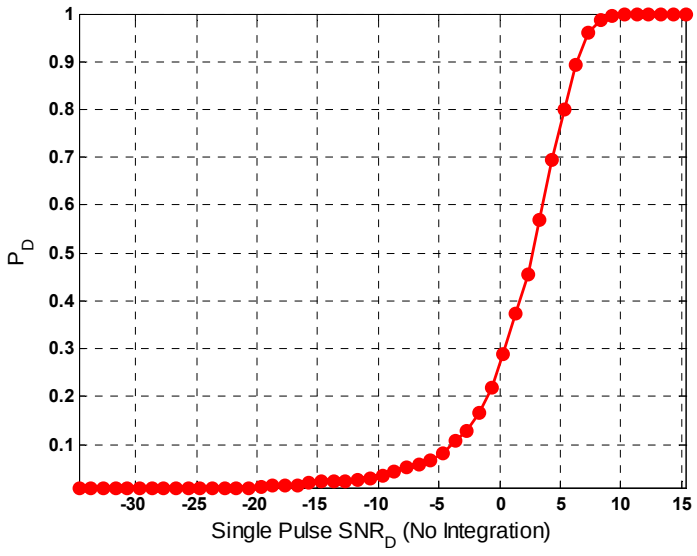

Figure 3.9: Baseline Detection Performance *Without* M-Code Signal Present

To correctly model M-Code signal presence during threshold determination, the number of M-Code realizations was set equal the number of *AWGN* realizations (1000 for $P_{FA} = 0.01$). Therefore, the M-Code was simulated by generating 1000 random binary sequences at each power level (-160 to -131 dBW). The only operating point considered for analyzing M-Codes interference effects is $P_D = 0.9$. Figure 3.10 shows radar detection performance with the M-Code signal present (red solid line) and baseline performance (blue dashed line) set to $P_D \approx 0.9$ using $SNR_D = 7.678$ dB.

Since the received radar return power is only -138 dBW, as calculated previously using (2.10), it was expected that the M-Code would impact P_D performance. The results in Fig. 3.10 are consistent with those presented in [6] and exhibit the expected

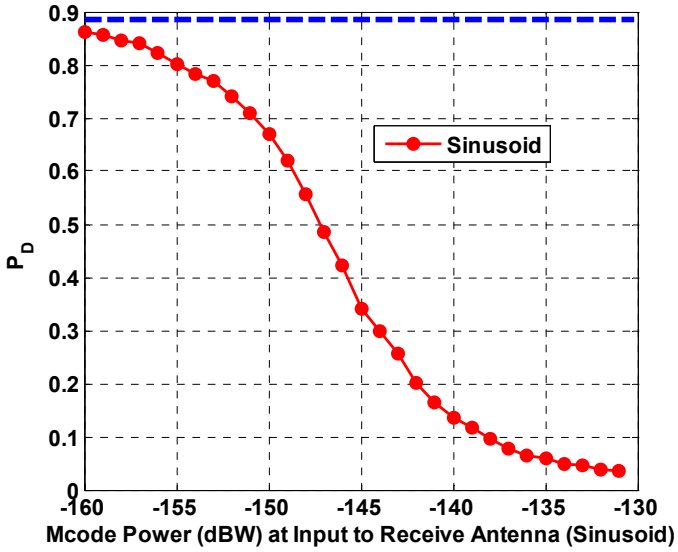

Figure 3.10: Detection Performance *With* M-Code Signal Present: Baseline Performance Set for $P_D \approx 0.9$ using $SNR_D = 7.678$ dB

degradation; P_D drops from baseline $P_D \approx 0.9$ performance to a value approaching $P_{FA} = 0.01$.

3.3.3 Radar Pulse Compression with M-Code Interference

Many practical radar systems, including the ARSR-4, use some form of pulse compression to improve range resolution. For completeness, this work considers both linear frequency modulation (LFM) and bi-phase Barker coded compression techniques. Although no real processing gain is expected due to pulse compression itself, i.e., increased immunity to interference and less P_D degradation, previous results in [6] indicate some residual improvement as a result of filter implementation and coloration. As previously explained, pulse compression effectively causes bandwidth expansion

under fixed pulse width constraints. Thus, the bandwidth of the IF2 filter is varied to accommodate the radar signal being considered as shown in Table 3.3. Note that the original 400 KHz bandwidth of the IF1 filter is sufficient to pass nearly 100% of the energy in the compressed waveforms and requires no modification.

Table 3.3: IF2 Filter Bandwidths

Type of Radar Signal	IF Bandwidth
Unmodulated Sinusoid	11 KHz
LFM	111 KHz
Bi-Phase Barker Coded	143 KHz

The goal when introducing pulse compression was to obtain approximately 10.0 dB (or greater) processing gain. Therefore, an up-chirped signal having a bandwidth of 111 KHz was chosen for the LFM pulse compression case. For the bi-phase Barker coded waveform, a Barker code of length 13 was used for phase modulation. Given the fundamental radar signal was changed, new baseline performances were established for each of the compression. Figure 3.11 provides baseline radar detection results for the unmodulated sinusoid, up-chirped LFM and bi-phase Barker coded signals. Consistent with results of [6], the improvement (higher P_D for given SNR_D) resulting from pulse compression is due solely to a change in correlator/detector output statistics resulting from filter coloration of the AWGN. Basically, the LFM and Barker coded reference waveforms used in the detector correlation process are less correlated with the filtered noise than the unmodulated sinusoid. This correlation effect yields a lower threshold value and corresponding increase in P_D for a given set of noise realizations.

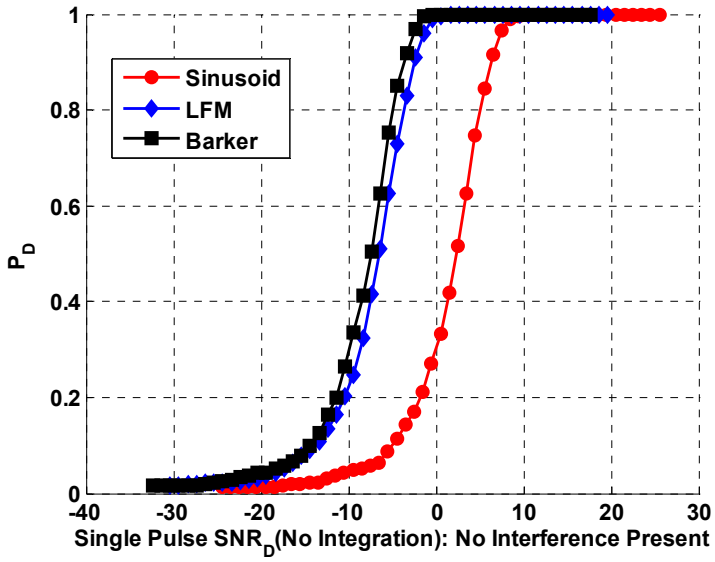

Figure 3.11: Baseline P_D vs SNR_D Prior to Introducing Interfering M-Code Signal (Unmodulated Sinusoid, LFM and Barker Coded Radar Pulses)

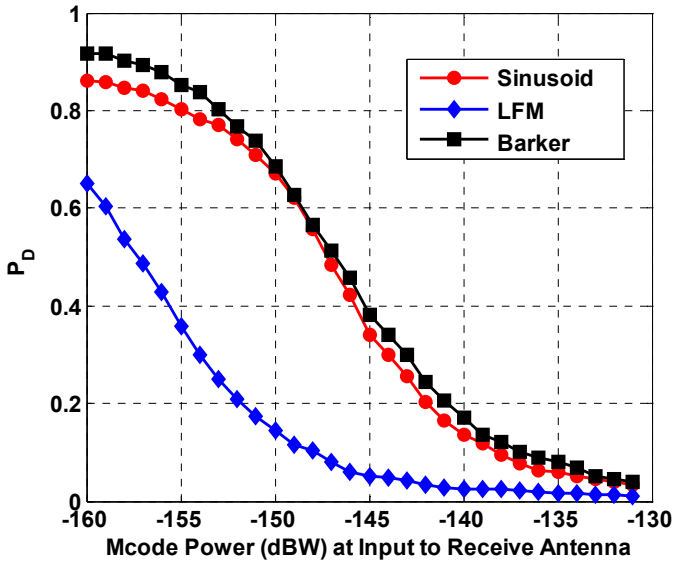

Figure 3.12: Effects of M-Code Signal on Baseline $P_D \approx 0.9$ for Unmodulated Sinusoid, LFM and Barker Coded Radar Pulse

After producing additional baseline performance results for the two pulse compression cases, the M-Code signal was introduced as in the unmodulated sinusoid case and interference effects analyzed. Effects of M-Code interference when pulse compression is employed are illustrated above in Fig. 3.12 where the appropriate SNR_D from Fig. 3.11 is used to achieve baseline $P_D \approx 0.9$.

The detection curves in Fig. 3.12 for pulse compression waveforms indicate 1) the bi-phase Barker coded waveform is slightly more robust than the unmodulated sinusoid while 2) the LFM waveform is considerably less tolerant to M-Code interference than both the Barker coded and unmodulated sinusoid waveforms. In addition to the noise colorization effects described earlier, these results and subsequent histogram analysis of correlator output statistics indicate that the IF filtered M-Code signal is somewhat more correlated with the LFM waveform than either the unmodulated sinusoid or Barker coded waveform. Figure 3.13 to 3.15 show normalized PDFs for statistical values listed in Table 3.4 and illustrate why results of Fig. 3.12 are obtained. For this PDF analysis, the test statistic values in Table 3.4 were collected using an M-Code received power of −150 dBW. As expected, the variance of $z_n(t) + z_{int}(t)$ and the variance of $z_{tot}(t)$ in Table 3.4 are equal for individual waveforms. However, the variances of $z_n(t) + z_{int}(t)$ for each of the three waveforms analyzed are *not* identical. As shown by Fig. 3.14, the LFM case possesses the highest variance in $z_n(t) + z_{int}(t)$ (the terms summed when setting the threshold of the three cases), resulting in a higher threshold setting for a given P_{FA} (fixed for all three figures). This elevated threshold yields a lower P_D in the LFM case, which

explains the poorer LFM performance in Fig. 3.12 compared to the Sinusoid and Barker performances.

For clarity in the figures, the threshold (z_T) is shown as a vertical dashed line, with fixed P_{FA} indicated as the shaded regions (area under curves) of the right-most tail of the $z_n(t) + z_{int}(t)$ PDFs in the figures, and P_D is represented by the region of $z_{tot}(t)$ PDF on the right-hand side of the threshold (slashed lines). To permit visual comparison, the PDFs are normalized by their peak value with the abscissa scales identical in all three figures.

Table 3.4: Single Pulse Test Statistics (M-Code Power of -150 dBW)

	Sinusoid		LFM		Barker	
Test Statistics	**mean**	**variance**	**mean**	**variance**	**mean**	**variance**
$Z_{int}+Z_n$	-8.23E-07	3.41E-10	2.15E-07	2.46E-09	-1.56E-06	3.64E-10
Z_{tot}	5.37E-05	3.41E-10	6.22E-05	2.46E-09	5.31E-05	3.64E-10
Threshold (Z_T)	4.63E-05		1.15E-04		4.43E-05	

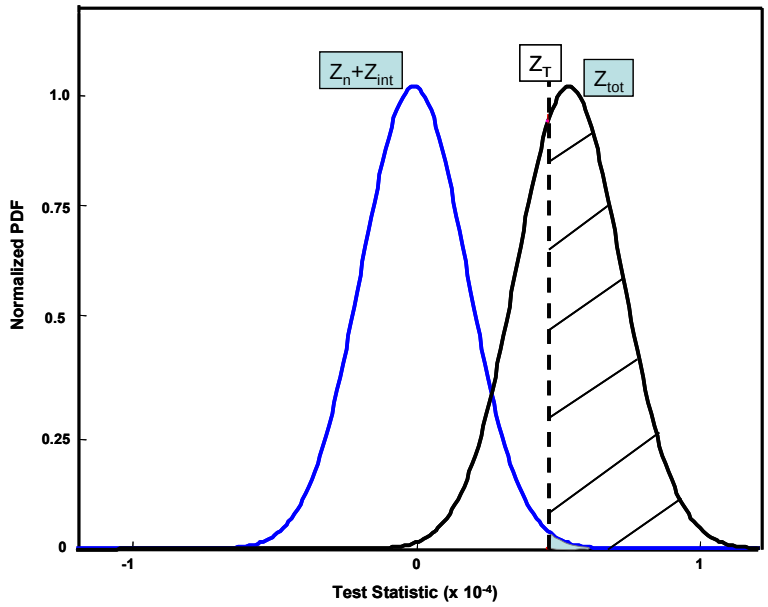

Figure 3.13: Sinusoid PDF Analysis Without Pulse Integration

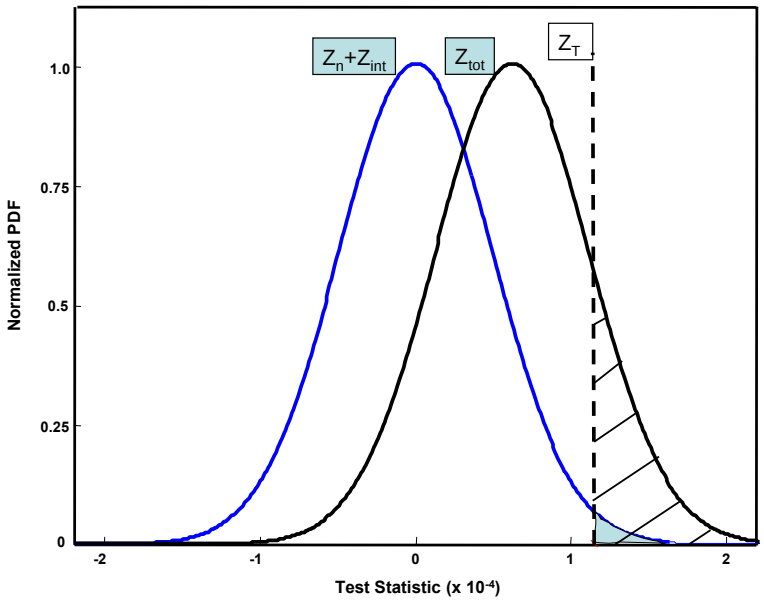

Figure 3.14: LFM PDF Analysis Without Pulse Integration

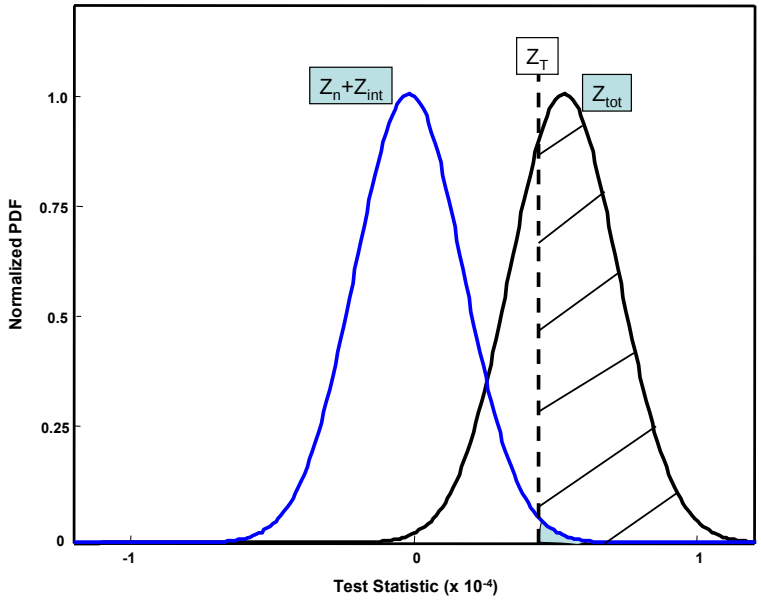

Figure 3.15: Barker PDF Analysis Without Pulse Integration

3.3.4 Radar Pulse Integration with M-Code Interference

Radar systems commonly employ some form of pulse integration to improve P_D. The number of pulses integrated in a given system is dependant on antenna beamwidth, the PRF and the scan time. In the case of the ARSR-4, eight pulses are integrated for detection purposes. To demonstrate the power of pulse integration in rejecting the effects of interfering signals, simulations were conducted using coherent integration of eight pulses (ARSR-4 parameter). For all pulse integration simulations, the radar return signal was generated using the simple sinusoid and the two introduced methods of pulse compression—LFM and 13-bit Barker code. New baseline (no interference present) detection results for the LFM waveform with pulse integration are shown in Fig. 3.17. Note that the x-axis is no longer "Single Pulse SNR_D," but rather, simply *"SNR_D"* (*SNR*

into the detector and incorporating the effects of pulse integration). The previously generated single pulse baseline LFM plot is included for comparison purposes in Fig. 3.16. As seen by comparing Fig. 3.16 and Fig. 3.17 results, approximately 8.0 dB of gain (reduction in required SNR_D to achieve given P_D) is realized with coherent pulse integration. Although not included here, this gain was obtained for all three radar waveforms considered and is consistent with theoretic improvement predicted by (2.16). Any disparity between simulated improvement and that of (2.16) could be directly attributed to AWGN condition imposed in deriving (2.16).

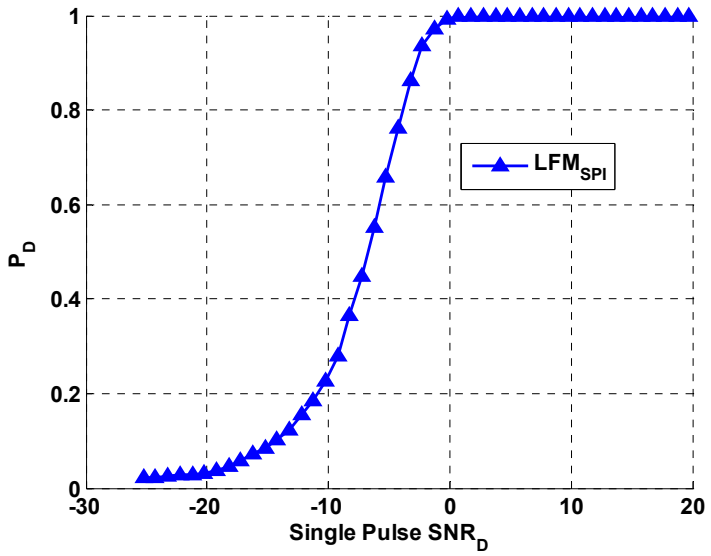

Figure 3.16: Baseline LFM P_D vs SNR_D Performance: No Pulse Integration and Interfering M-Code Signal Not Present

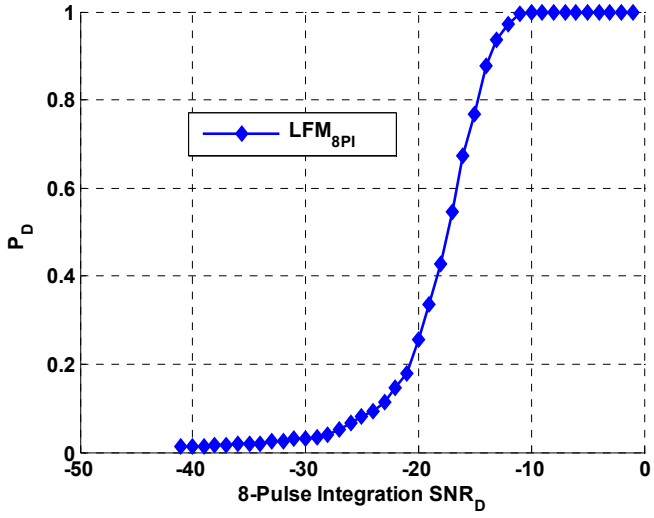

Figure 3.17: Baseline LFM P_D vs SNR_D Performance: 8 Pulses Integrated and Interfering M-Code Signal Not Present

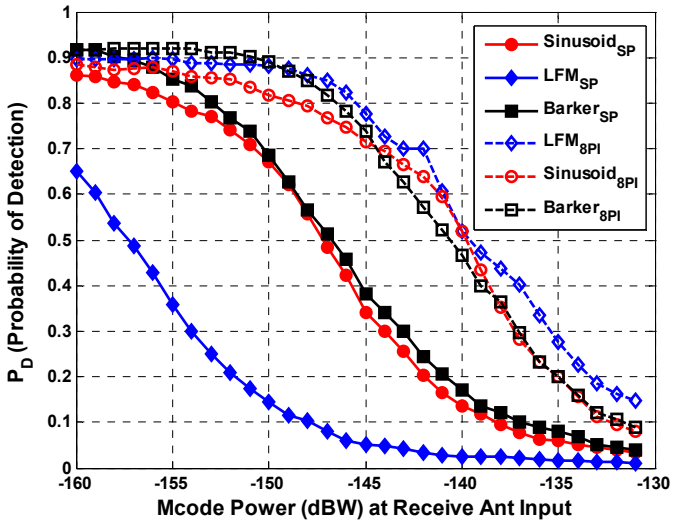

Figure 3.18: Detection Performance Degradation from Baseline $P_D \approx 0.9$ for Pulse Integration and M-Code Interfering Signal Present

Detection performance degradation results for pulse integration with the interfering M-Code signal present are shown in Fig. 3.18. As indicated, the unmodulated sinusoid and Barker coded waveform achieved nearly 8.0 dB gain as expected for pulse integration. On the other hand, the LFM waveform shows nearly 18.0 dB improvement in detection performance. This disparity between the theoretical and simulated results is once again attributed to filter 'coloration' effects on the *AWGN* and the M-Code interferer. When the simulation was rerun using an independent realization of *AWGN* to replace the M-Code signal, the theoretically calculated gain of approximately 9.0 was obtained (results not shown).

To support pulse integration results displayed in Fig. 3.18, histogram analysis of correlator output statistics is performed again as it was in Section 3.3.3 when no pulse integration was employed. For this PDF analysis, the test statistic values in Table 3.5 were collected using a received M-Code power of −150 dBW. The data in Table 3.5 and corresponding Figs. 3.19 to 3.21 show that the variance of $z_n(t) + z_{int}(t)$ and the variance of $z_{tot}(t)$ are again equal for individual waveforms. However, unlike results for no pulse integration, the variances of $z_n(t) + z_{int}(t)$ for each of the three waveforms analyzed here are now quite similar. This similarity yields the comparable P_D results shown in Fig. 3.18 for pulse integration.

As in the previous section, in Figs. 3.19 to 3.21 the threshold (z_T) is shown as a vertical dashed line, with fixed P_{FA} indicated as the shaded regions (area under curves) of the right-most tail of the $z_n(t) + z_{int}(t)$ PDFs in the figures, and P_D is represented by the region of $z_{tot}(t)$ PDF on the right-hand side of the threshold (slashed lines). To permit

visual comparison, the PDFs are normalized by their peak value with the abscissa scales identical in all three figures.

Table 3.5: 8-Pulse Integrated Test Statistics (M-Code Power of -150 dBW)

	Sinusoid		LFM		Barker	
Test Statistics	**mean**	**variance**	**mean**	**variance**	**mean**	**variance**
$Z_{int}+Z_n$	-2.12E-05	1.05E-06	-8.10E-06	1.30E-06	-1.58E-06	1.03E-06
Z_{tot}	3.50E-03	1.05E-06	4.00E-03	1.30E-06	3.50E-03	1.03E-06
Threshold (Z_T)	2.50E-03		2.60E-03		2.30E-03	

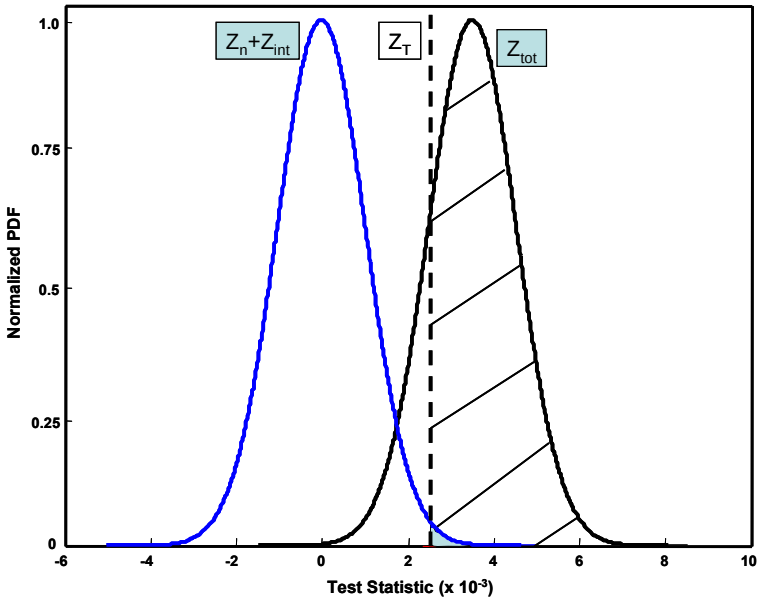

Figure 3.19: Sinusoid PDF Analysis With 8-Pulse Integration

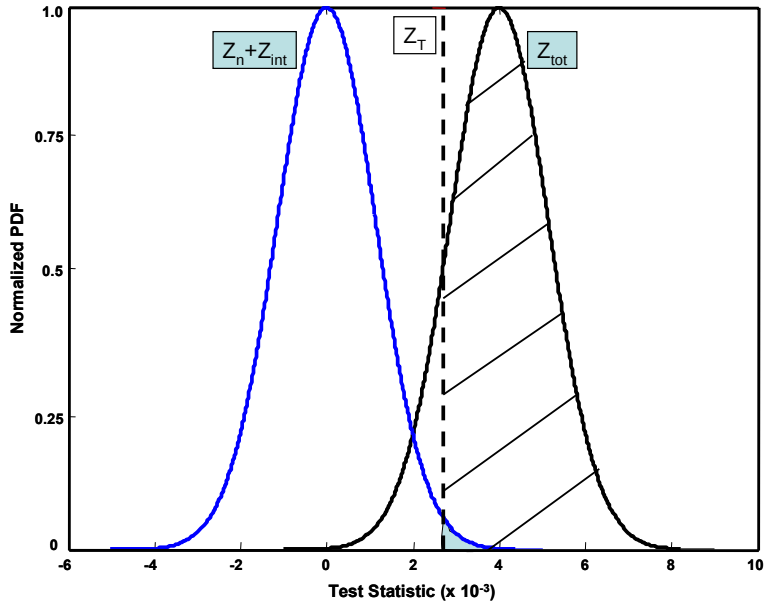

Figure 3.20: LFM PDF Analysis With 8-Pulse Integration

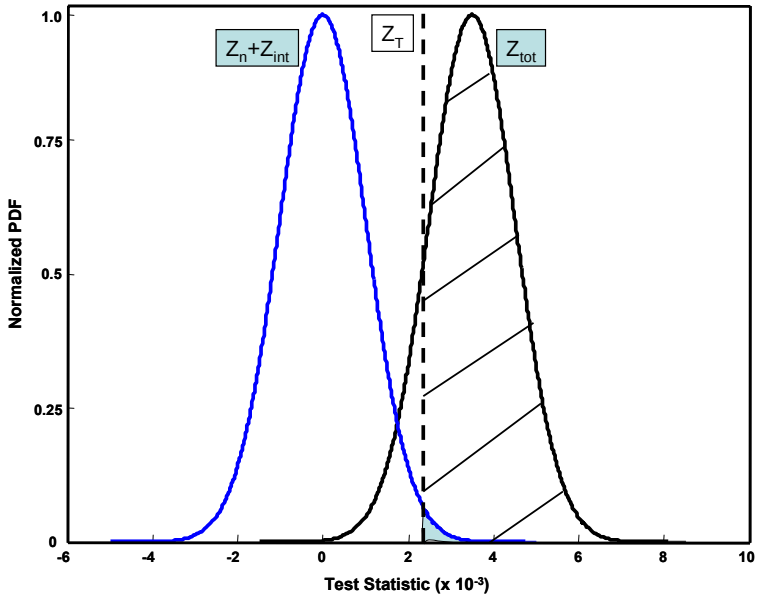

Figure 3.21: Barker PDF Analysis With 8-Pulse Integration

With the exception of the pulse compression results presented here, the M-Code simulation results in this chapter are consistent with those obtained under similar conditions in [6]. Since the work in [6] did not properly incorporate the varied bandwidths of the IF2 filter which correspond respectively to the three different radar signals analyzed, the work in [6] recorded the LFM case out-performing the Sinusoid case. In actuality, as Figures 3.12 and 3.18 show, the Sinusoid case out-performs the LFM case, in terms of probability of detection, when pulse integration is not employed.

3.4 UWB Interference Analysis

The focus now shifts to characterizing UWB interference effects on radar detection performance. Once again, the basic radar model of Fig. 3.1 is used with many of simulation parameters remaining the same as used for M-Code characterization. The intent is not to compare UWB and M-Code degradation effects head-to-head. Rather, the idea is to present a robust radar model and analyze its detection performance while under the influence of two distinct interfering signal structures, one carrier based (M-Code) and one carrierless (UWB).

As in the M-Code analysis, it is advantageous to first define simulation assumptions and parameters before introducing UWB interference analysis results. Again, the simulation scenario is designed to invoke worst case radar detection performance. The assumed UWB simulation geometry is shown in Fig. 3.22 on the next page and summarized as follows [24]:

1. *Returned radar energy is from a stationary airborne point target located at the maximum required detection range.* Thus, maximum propagation path loss occurs, there is no Doppler shift and the return signal is received at minimum detectable power levels.

2. *Initial simulated radar processing is for single pulse detection.* These results represent baseline performance and do not include benefits of pulse compression (range resolution enhancement) or pulse integration (processing gain). Pulse compression and integration are subsequently addressed.

3. *The interfering UWB signal is received along the same line-of-sight as the target return signal.* The target return and interfering signals experience identical (maximum) antenna gain upon reception.

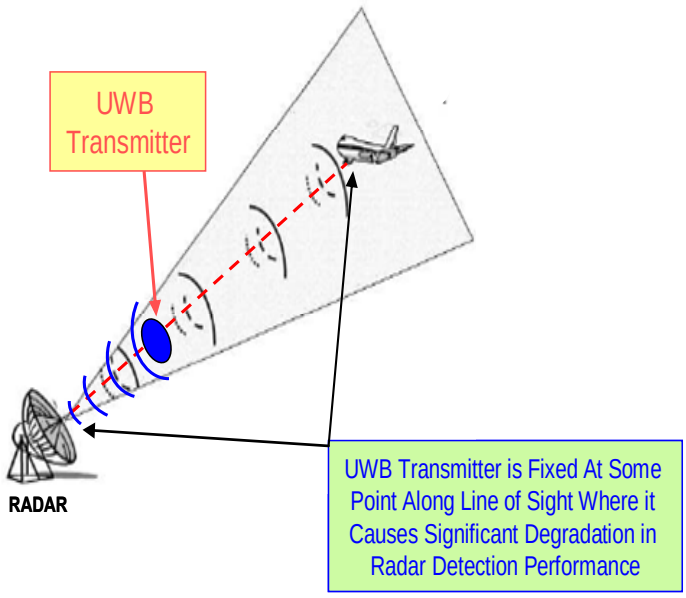

Figure 3.22: UWB Simulation Geometry

4. *The radar carrier frequency and peak spectral response of UWB interfering signals are coincident.* Thus, maximum received interfering signal power is processed.

5. *The propagation channel is additive white Gaussian noise (AWGN).*

6. *Interfering UWB signals are continuously received during threshold determination.* The receiver threshold is set to ensure a constant false alarm rate (CFAR) is maintained while both interfering signals and AWGN are present.

7. *The radar receiver bandwidths (RF and IF) are matched to the radar signal under consideration.* The bandwidths are established as the -4 dB bandwidth of the radar signal. Waveforms considered include an unmodulated sinusoid, LFM and bi-phase Barker coded, all of which are considered narrowband relative to the interfering UWB signals considered.

With the baseline results of P_D versus SNR_D (for a single pulse sinusoid) in place and simulation assumptions clarified (Fig. 3.4 and Fig. 3.9), a P_D level is selected, SNR_D is fixed (thus fixing average signal and noise power before the detector), and the UWB signal is added at the receive antenna. As for the M-Code interference case, the process depicted in Fig. 3.6 was used for selecting P_D and determining required SNR_D before the interferer UWB signal is added.

With the UWB signal present, the return signal power is held constant (at the minimum received power level for a target at the maximum required detection range) and the noise power is varied to obtain the desired SNR_D value (or equivalently, the desired P_D). This procedure ensures the relative power levels between the radar return signal and

the UWB signal are accurately modeled. The power relationship is maintained by calculating the radar return signal power and the interfering signal power at the receive antenna. As in the previous M-Code analysis, the target return power was held constant a -138 dBW as derived in (3.4). Given target return power is fixed, the noise power is adjusted in the UWB simulations to achieve the desired SNR_D. For each desired SNR_D, the unit-power noise samples are scaled by a gain factor given by (3.5).

Since noise power changes for each desired SNR_D, a new detection threshold value is required to maintain a constant P_{FA}. The process described previously for determining the threshold value is used repeatedly for each SNR_D value. At this point, the received interfering UWB power is varied to characterize how the interferer affects the established P_D. The UWB signal is generated using (2.4) center frequency of 7.0 GHz. Once again, the goal is to effectively simulate a filtered $1/\tau$ (approximately 11.0 KHz for the unmodulated sinusoid) bandwidth portion of the UWB BPPM waveform where both the peak signal response and filter are centered at the IF2 filter center frequency of 400 KHz.

The following process was employed for generating the filtered UWB interfering signal. The UWB signal was first generated at a center frequency of 7.0 GHz and then filtered by the RF/IF2 filter in Fig. 3.1 centered at 10.0 MHz at a bandwidth of 250 KHz. Finally, the filtered UWB signal is down-converted to the center frequency of the IF2 filter located at 400 KHz. It is assumed that this procedure is consistent with down-conversion and filtering processes found in radar receivers and effectively captures the maximum UWB signal power. Once the UWB signal is filtered at IF2, it has the desired

$1/\tau$ bandwidth of approximately 11.0 KHz. As shown in Fig. 3.1, the UWB signal is added to the radar return signal at the receive antenna input. The composite received waveform experiences received antenna gain prior to RF/IF1 filtering, down-conversion, IF2 filtering and subsequent matched filter detection.

Unlike the M-Code case where the separation distance between the M-Code transmitter and the radar receiver was fixed and the M-Code received power varied in accordance with parameters in Table 2.1, the UWB transmitter is modeled as being located anywhere on the line-of-sight between the radar and target as shown in Fig. 3.22. Initial simulation results in this work were obtained by varying the received UWB interfering power until "significant" degradation occurred in detection performance. *Significant* is defined as a 10% or greater decrease in baseline P_D. Once the appropriate received interfering power range was determined, corresponding radar/UWB separation distance (range) was calculated using Friis transmission of (2.14). The loss factor of (2.15) was calculated by finding the difference in power at the RF/IF2 filter output at 7.0 GHz (UWB center frequency) and UWB power levels at the receive antenna input. Using this method, the UWB power range (in the 250 KHz bandwidth of the RF/IF1 filter) at the receive antenna input was determined to be − 141 dBW to − 112 dBW. Applying the maximum receive antenna gain of 40.91 dB from Table 3.1, the UWB signal power prior to the RF/IF1 filter ranges from − 99.09 dBW to 70.09 dBW. All UWB simulated results that follow, excluding baseline cases when no UWB interference is present, are based on this power range. Separation distance (meters) is shown along the top of all UWB simulation plots.

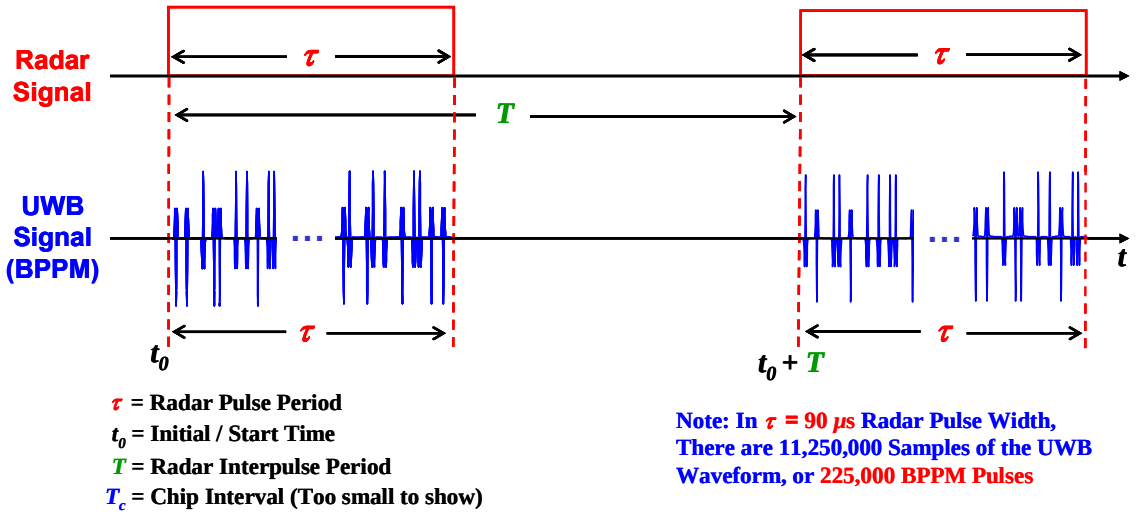

Figure 3.23: UWB Pulses Gating Example

3.4.1 UWB Interference Gating

The UWB interference gating process is similar to that used for M-Code analysis. However, for the simulation parameters considered there are hundreds-of-thousands of random BPPM pulses present in every pulse duration τ as illustrated in Fig. 3.23 above. Thus, pulse gating is not as critical for obtaining reliable UWB results. However, the effects of pulse gating are incorporated in the UWB signal generation such that a random starting phase (position within first BPPM symbol) is induced. Figure 3.23 illustrates the UWB pulse gating concept.

3.4.2 UWB Interference Effects

For a worst case scenario, it is assumed that the UWB transmitter transmits continually. Thus, when the radar sets the threshold the UWB signal is present as a

source of interference. For the remaining simulations, the interfering signal is individually added to the noise and is present during threshold determination.

The next step was to investigate the effects of having UWB interference present during threshold determination. For comparison, baseline detection results of Fig. 3.9 without the UWB interference present are reintroduced on the following page in Fig. 3.24. Using a fixed SNR_D to achieve a specific P_D, the UWB interference was introduced to ascertain the interference effects on baseline P_D performance. The incident received UWB power was varied from −141 to −112 dBW given this was previously established as the range causing significant P_D degradation. The P_D was then estimated as in the baseline case except now the UWB interference was present during threshold determination. Figure 3.6 illustrates the process of selecting a P_D from a baseline performance plot and of choosing the corresponding SNR_D. The signal and noise powers are then fixed to achieve this SNR_D level and the UWB interfering signal is introduced.

To correctly model UWB signal presence during threshold determination, the number of UWB signal realizations was set equal the number of *AWGN* realizations (1000 for $P_{FA} = 0.01$). Therefore, the UWB signal was simulated by generating 1000

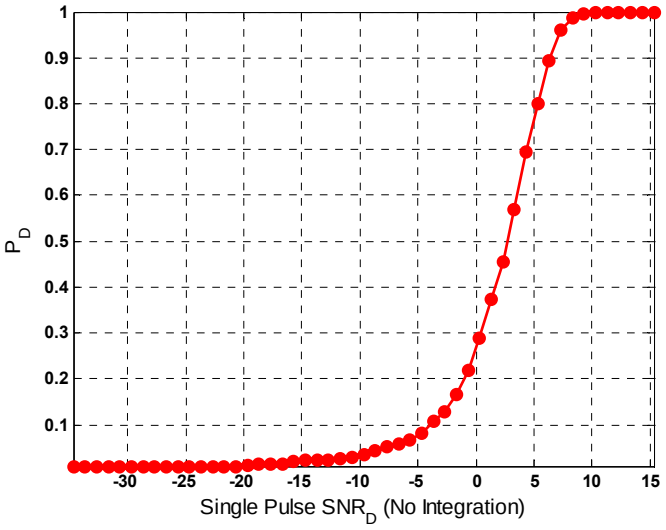

Figure 3.24: Baseline Detection Performance *Without* UWB Signal Present

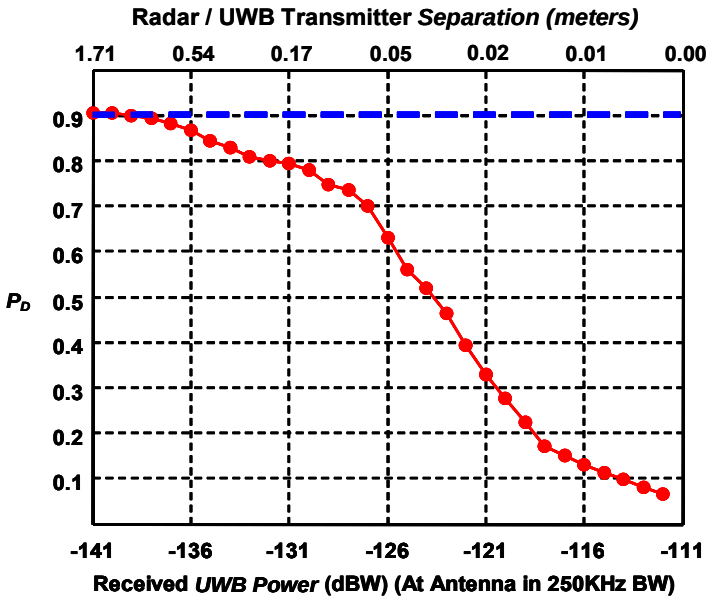

Figure 3.25: Detection Performance *With* UWB Signal Present: Baseline Performance Set for $P_D \approx 0.9$ using $SNR_D = 7.678$ dB

random BPPM waveforms at each power level (−141 dBW to −112 dBW.). As in the M-Code case, the only operating point considered for analyzing UWB interference effects is $P_D = 0.9$. Figure 3.25 shows radar detection performance with the UWB signal present (red solid line) and baseline performance (blue dashed line) set to $P_D \approx 0.9$ using $SNR_D = 7.678$ dB.

It is important to remember here that the degradation illustrated in Fig. 3.25 is somewhat arbitrary in that the UWB received signal power was varied until such "significant" degradation was observed. These power levels were then mapped via Friis transmission to the corresponding radar/interferer separation distances shown on top of the plot. This process is clearly different from the M-Code case where radar/interferer separation distance is fixed and received power level variation is specified per operational parameters.

3.4.3 Radar Pulse Compression with UWB Interference

As in the M-Code analysis of Section 3.3.3, radar detection performance with pulse compression and the UWB interfering signal is considered next. Baseline detection results of Fig. 3.11 without the UWB interference present are reintroduced here in Fig. 3.26 for comparison.

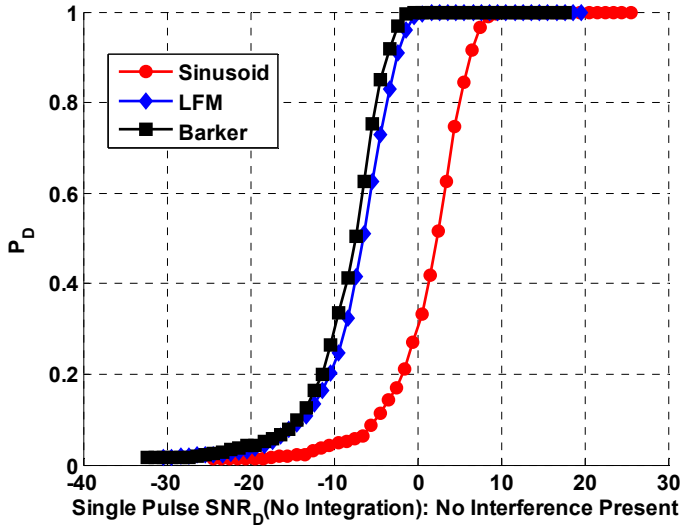

Figure 3.26: Baseline P_D vs SNR_D Prior to Introducing Interfering UWB Signal (Unmodulated Sinusoid, LFM and Barker Coded Radar Pulses)

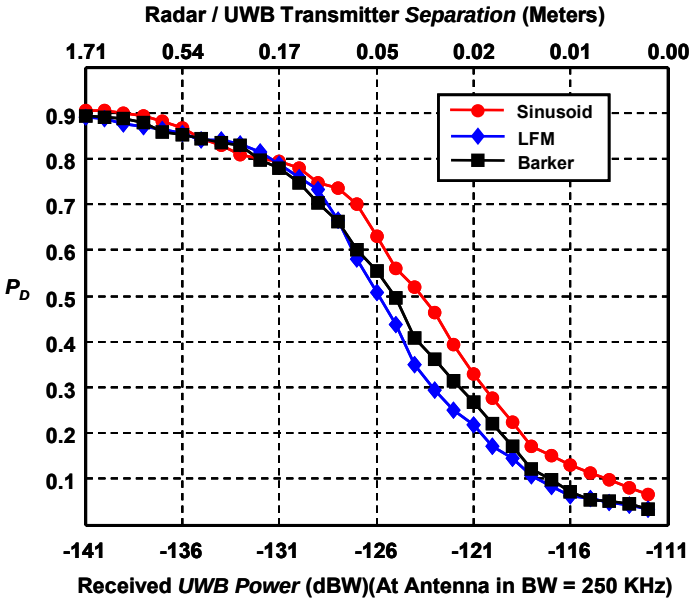

Figure 3.27: Effects of UWB Signal on Baseline $P_D \approx 0.9$ for Unmodulated Sinusoid, LFM and Barker Coded Radar Pulse

Detection results for a radar incorporating pulse compression are presented above in Fig. 3.27 and indicate marginal change relative to the unmodulated sinusoidal pulse. Although the compressed waveforms perform somewhat poorer (about 2.0 to 3.0 dB poorer near $P_D \approx 0.5$), it is important to note the separation distances on the top x-axis scale of the plot in Fig. 3.27 reveals that the UWB transmitter must be within 0.5 meter of the radar to "significantly" degrade detection performance, regardless of waveform type.

3.4.4 Radar Pulse Integration with UWB Interference

As in the M-Code analysis of Section 3.3.4, radar detection performance with pulse integration and the UWB interfering signal is considered next. For comparison, baseline detection results of Fig. 3.16 and Fig. 3.17 without the UWB interference present are reintroduced here in Fig. 3.28 and Fig. 3.29, respectively.

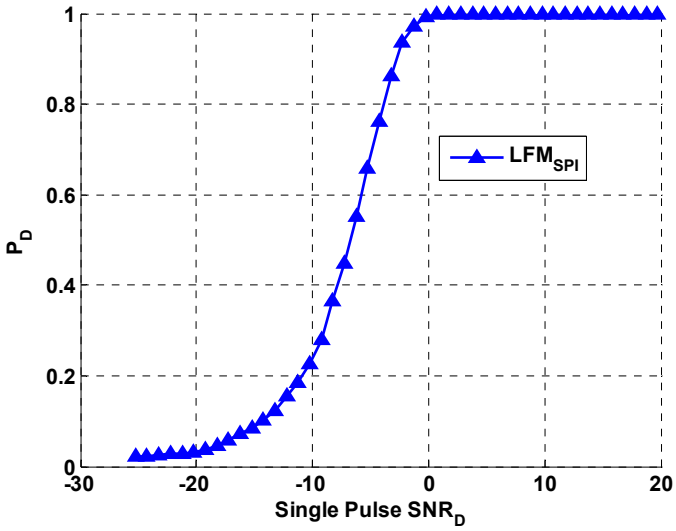

Figure 3.28: Baseline LFM P_D vs SNR_D Performance: No Pulse Integration and Interfering UWB Signal Not Present

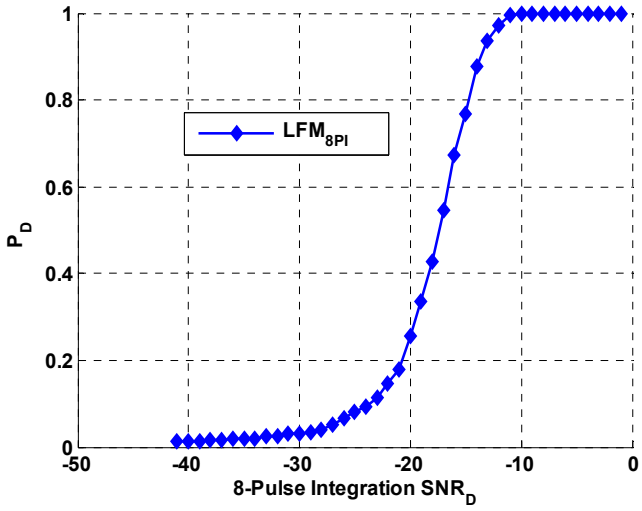

Figure 3.29: Baseline LFM P_D vs SNR_D Performance: 8 Pulses Integrated and Interfering UWB Signal Not Present

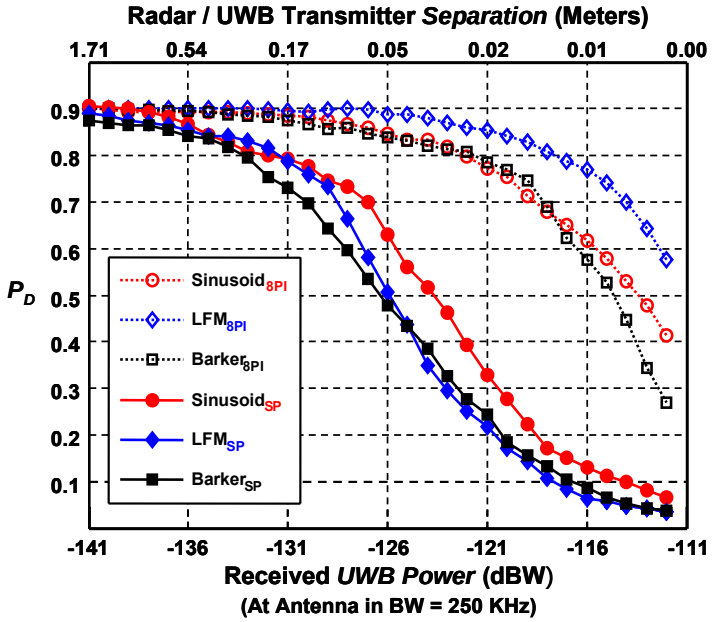

Figure 3.30: Detection Performance Degradation from Baseline $P_D \approx 0.9$ for Pulse Integration and UWB Interfering Signal Present

Results in Fig. 3.30 indicate that with coherent pulse integration, 1) the unmodulated sinusoidal wavform realized approximately 11.0 dB gain, 2) the bi-phase Barker coded waveform realized approximately 12.0 dB gain, and 3) the LFM waveform was somewhat higher with nearly 15.0 dB gain. As with the M-Code case, the expected improvement is on the order of that predicted by (2.16), which is 8.0 dB gain for all cases. The disparity between simulated improvement and that of (2.16) is believed to be directly attributable to the AWGN condition imposed in deriving (2.16). Simulated results presented here include filter 'coloration' effects on both the *AWGN* and interfering signal. With pulse integration, the previous 0.5 meter separation distance which caused "significantly" degraded detection performance has been further reduced 0.05 meters.

3.5 Summary

This chapter provides simulation methodology, results and analysis of GPS M-Code and modern UWB signal effects on radar detection performance. Discussion is provided on four simulation phases, including: 1) baseline detection performance with no interference present, 2) detection performance with the interference present during threshold determination, 3) detection performance using radar pulse compression with interference present, and 4) detection performance using coherent pulse integration with interference present. One basic radar receiver design was used in which both the radar return signal and interference signals are filtered at both the RF/IF1 and IF2 levels.

Simulated M-Code results indicate that for the minimum specified power level of −160 dBW, the M-Code signal has minimal effect on radar detection capability. However, for a single pulse radar system with or without pulse compression, radar

detection performance is significantly degraded when the M-Code signal is at its maximum power level of −131 dBW. These results are consistent with those of previous work in [6].

Simulated UWB results indicate that at the minimum received interfering power level of −141 dBW, the UWB BPPM signal has little effect on radar detection performance. However, in a single pulse radar system with or without pulse compression, detection performance is significantly (less than or equal to 10%) degraded when the received UWB power −112 dBW. Based on this range of power levels, and the maximum transmitted UWB signal power authorized by the FCC, the separation distance between the radar receiver and UWB transmitter must be less than 0.5 meters (or 0.05 meters with eight pulses integrated) before significant degradation occurs in radar detection capability.

In both the M-Code and UWB interfering cases, coherent integration of eight pulses provides at least 8.0 dB gain (reduction in required SNR to achieve specified P_D) in radar detection performance, with greater than 8.0 dB realized in some cases. The improvement above and beyond what is commonly predicted for coherent integration of n pulses (an n-fold improvement in SNR is predicted for coherent integration over AWGN channel) is directly attributable to noise and signal coloration effects induced as a result of the filtering implemented in the simulations. This coloration effectively changes the correlator output statistics which dictate detection performance.

IV. Conclusions

4.1 Conclusions

This research presented the theory, modeling and simulation results characterizing radar detection performance in the presence of two modern interference waveforms, namely the GPS military signal (M-Code signal) and a direct sequence ultra wideband (DS-UWB) waveform meeting outdoor emission restrictions imposed by the Federal Communications Commission (FCC). Modeling and simulation is based on presenting a worst case scenario to the radar receiver and based on the following key assumptions:

- Returned radar energy is from a stationary airborne point target at the maximum target detection range. This assumption results in the lowest (worst-case) return power.
- Target returns and interfering signals are received along a direct line-of-sight to the radar and experience identical (maximum) gain upon reception.
- Detection threshold is set under two conditions: 1) for baseline simulations with *no interference present*, the threshold is set with only AWGN present, and 2) for all other simulations *with interference present*, the threshold is set with AWGN and the interfering signal present.
- Average incident M-Code was varied across the proposed range of −160 to −130 dBW with the radar receiver/M-Code transmitter separation distance maintained constant.
- Average incident DS-UWB power was varied across a range of −141 dBW to −112 dBW, a range determined to induce severe (approximately 10% or

greater) detection performance degradation. These incident DS-UWB power levels are obtained by fixing transmitted power to the maximum level specified by the FCC and varying the radar receiver/DS-UWB transmitter separation distance.

- Additional assumptions common to M-Code and DS-UWB analysis can be found in Chapter 3.

For a single pulse radar system, M-Code results indicate that the M-Code signal minimally impacts radar detection capability at the *minimum* specified power level of −160 dBW when both RF/IF1 and IF2 filtering effects are simulated; P_D decreased by approximately 4% for the unmodulated sinusoidal pulse. At the *maximum* specified M-Code power of −131 dBW, radar detection performance was more seriously degraded; both with and without pulse compression, P_D decreased to a value approaching P_{FA}. With few exceptions, the M-Code interference results presented in this work are shown consistent to previous results in [6] and [7]. For the same single pulse radar system, DS-UWB interference results showed virtually no degradation in detection performance at the minimum operating power level of −141 dBW, independent of radar waveform type. As the interfering power level increased to the maximum level of −112 dBW, detection performance dropped to a level approaching P_{FA}. Using maximum authorized transmitted DS-UWB power, these power levels correspond to radar receiver/DS-UWB transmitter separation distances of 1.71 meters for −141 dBW to less than 0.5 meters for −112 dBW. Taking into consideration all modeling and simulation constraints imposed by this work, it is concluded that given a DS-UWB transmitter operating at maximum

authorized power levels, the DS-UWB transmitter would have to be located within approximately 1.0 meter of the radar receiver to cause severe degradation in radar detection performance.

For a radar system employing coherent pulse integration to improve pre-detection SNR (and thus detection capability) results of this work are as expected and indicate improvement relative to the single pulse system. A system that coherently integrates eight pulses (consistent with ARSR-4 operation) was simulated and showed at least 8.0 dB improvement near the mid-range of specified M-Code powers for all three radar waveforms considered. In some cases, improvement greater than 8.0 dB was realized and it was determined that the added improvement (above what is expected for coherent pulse integration over an AWGN channel) was directly attributable to filter coloration effects on the AWGN and radar signals. However, P_D once again decreased to a value approaching P_{FA} when the M-Code was at its maximum specified power of −131 dBW; integration of only eight pulses was insufficient to completely restore detection performance across the entire proposed range of received M-Code power levels. Simulated DS-UWB interference results with pulse integration exhibited the same behavior as the M-Code case, once again providing at least 8.0 dB improvement near mid-range of the DS-UWB power range considered. Here again, the coloration of the noise and interference signals resulting from filtering attributed the higher than expected gains. As expected, pulse integration improved detection performance and thereby decreased the required separation distance required to yield significant degradation; less than 0.05 meters of separation was required when eight pulses were integrated.

It is reiterated that all results presented in this work were obtained for *worst-case* detection scenarios (from the radar receiver's perspective). When possible, ARSR-4 parameters were used to ensure the results reasonably extend beyond the realm of academia. Further detailed modeling of the ARSR-4 radar system, to include using non-linear frequency modulation (NLFM) pulse compression, is necessary before directly applying these results and concluding with certainty that the M-Code and DS-UWB signals considered will or will not significantly impact ARSR-4 detection performance.

4.2 Recommendations for future research

As previously noted, many assumptions were included when constructing the models used in this research. Therefore, the following list of recommendations chould be explored for follow-on research:

1. The simulations should be run using lower, more practical false alarm rates in the neighborhood of 10^{-5} to 10^{-6}. Due to computational resource limitations, simulations for this research were run using a $P_{FA} \approx 10^{-2}$.
2. Radar technology is migrating toward architectures/networks having multiple receivers and transmitters. This research could be extended to include Multiple Input Multiple Output (MIMO) type systems versus the single transmitter/receiver system considered here.
3. Simulation parameters could be modified to simulate other radar systems, such as aircraft systems operating in the 9.0 to 10.0 GHz range. This research simulated system parameters consistent with those of the ARSR-4.

4. The effects of other modern signals (communication, navigation, etc.) on radar detection performance could be evaluated. In fact, there are many other UWB waveforms other than the Bi-Orthogonal Pulse Position Modulation (UWB BPPM) analyzed here. The model developed here allows virtually any interfering waveform to be easily incorporated and its effect on detection performance analyzed.
5. The radar system could be modeled and analyzed using alternate detection and estimation strategies. Figure 3.3 illustrated how threshold determination was based on "signed" matched filter output test statistics. Systems employing various forms of energy detection (test statistics based component magnitudes, squares, etc.) could be evaluated.

Bibliography

1. National Academy of Public Administration and National Research Council, *The Global Positioning System: Charting the Future*, Summary Report, Washington, D.C., 1995.

2. Clabaugh, D. J. "Characterization of Ultra Wide Band Multiple Access Performance Using Time Hopped-Biorthogonal Pulse Position Modulation." Wright-Patterson AFB, OH. AFIT/GE/ENG/04.

3. "First Report and Order: Revision of Part 15 of the Commission's Rules Regarding Ultra-wideband Trans-mission Systems," FCC, Apr. 2002.

4. Navstar GPS Joint Program Office (JPO). *Navstar GPS Military-Unique Space Segment/User Segment Interfaces*. Interface Control Document. El Segundo, CA: GPS JPO, 2001.

5. Enge, Per and Pratap Misra. *Global Positioning System: Signals, Measurements, and Performance*. Lincoln MA: Ganga-Jamuna Press, 2001.

6. Wruck, Dean E. "GPS M-Code Signal Modeling for Radar Receiver Characterization." Wright-Patterson AFB, OH. AFIT/GE/ENG/04-25.

7. Yang, Jae. "The Effects of GPS M-Code On Radar Detection." Wright-Patterson AFB, OH. AFIT/GE/ENG/03-20.

8. Anon. *Fact Sheet: U.S. Global Positioning System Policy*. Presidential Directive. Washington, D.C.: The White House, Office of Science and Technology Policy, National Security Council, 29 March 1996.

9. Anderson, Jon M. and David J. Lucia. "Analysis and Recommendation for the Reuse of the L1 and L2 GPS Spectrum." *Proceedings of ION GPS-98* . Alexandria, VA: Institute of Navigation, 1998.

10. Barker, Brian C. and others. "Details of the GPS M Code Signal." *Proceedings of the Institute of Navigation, 2000 National Technical Meeting*. Alexandria VA: Institute of Navigation, 2000.

11. Clabaugh, D.J., et.al, "UWB Multiple Access Performance Using TH-PPM with Biorthogonal Signalling," IEEE Conference of Ultra Wideband Systems and Technologies, Reston, VA, 16-19 Nov 2003.

12. J. Padgett, "Coexistence of UWB and Legacy Narrow-band System," Telecordia Technologies, Contract MDA972-02-C-0056, February, 2003.

13. A. Swami, B. Sadler and J. Turner, "On the Coexistence of Ultra-Wideband and Narrowband Radio Systems" Military Communications Conference, MILCOM 2001, Vol. 1, pp. 16-19, October, 2001.

14. *Instruction Book, Field Maintenance, ARSR-4 System, Type FA-10331, Sections 1-10,* Technical Instruction TI-6340.23, Baltimore MD: Westinghouse Electric Corporation, December 1999.

15. Kaplan, Elliott D. *Understanding GPS, Principles and Applications*. Boston, MA: Artech House Inc., 1996.

16. Holmes, J. K. and S. Raghavan. "GPS Signal Modernization Update Summary." *Proceedings of ION 58th Annual Meeting/CIGTF 21st Guidance Test Symposium*. Alexandria VA: Institute of Navigation, 2002.

17. Betz, John W. "Analysis of M Code Interference with C/A Code Receivers." *Proceedings of ION 2000 National Technical Meeting*. Alexandria VA: Institute of Navigation, 2000.

18. Stimsom, George W. *Introduction to Airborne Radar* (Second Edition). Raleigh, NC: SciTech Publishing Inc., 1998.

19. Hovanessian, S.A. *Radar System Design and Analysis*. Norwood MA: Artech House, Inc., 1984.

20. Levanon, Nadav. *Radar Principles*. New York NY: John Wiley and Sons, Inc., 1988.

21. Skolnik, Merrill I. *Introduction to Radar Systems* (Third Edition). New York, NY: McGraw Hill, 2001.

22. Betz, John W. "The Offset Carrier Modulation for GPS Modernization." *Proceedings of the Institute of Navigation, 1999 National Technical Meeting*. Alexandria, VA: Institute of Navigation, 1999.

23. National Telecommunications and Information Administration. *U.S. Draft Proposal for WRC 2003* . Proposal. Washington D.C.: NTIA, 2002.

24. Backscheider, R. J., M. A. Temple, D. E. Wruck and T. B. Hale. "Characterization of Radar Detection Performance in the Presence of Modern Signal Interference." *Proceedings of the IEEE First International Waveform Diversity Conference*. Edinburgh, Scotland: Caledonian Hotel, 2004.

25. Balanis, Constantine A., *Antenna Theory: Analysis and Design,* (2nd Edition), NY: John Wiley & Sons, 1997.

REPORT DOCUMENTATION PAGE

Form Approved
OMB No. 074-0188

1. REPORT DATE *(DD-MM-YYYY)*	2. REPORT TYPE	3. DATES COVERED *(From – To)*
10-12-2004	**Master's Thesis**	Jan 2004 – Dec 2004

4. TITLE AND SUBTITLE

ULTRA WIDE BAND SIGNAL MODELING FOR RADAR RECEIVER CHARACTERIZATION

5a. CONTRACT NUMBER

5b. GRANT NUMBER

5c. PROGRAM ELEMENT NUMBER

6. AUTHOR(S)

Backscheider, Robert, J., Second Lieutenant, USAF

5d. PROJECT NUMBER

5e. TASK NUMBER

5f. WORK UNIT NUMBER

7. PERFORMING ORGANIZATION NAMES(S) AND ADDRESS(S)
Air Force Institute of Technology
Graduate School of Engineering and Management (AFIT/EN)
2950 P Street, Building 640
WPAFB OH 45433-8865

8. PERFORMING ORGANIZATION REPORT NUMBER

AFIT/GE/ENG/04-28

9. SPONSORING/MONITORING AGENCY NAME(S) AND ADDRESS(ES)

N/A

10. SPONSOR/MONITOR'S ACRONYM(S)

11. SPONSOR/MONITOR'S REPORT NUMBER(S)

12. DISTRIBUTION/AVAILABILITY STATEMENT

APPROVED FOR PUBLIC RELEASE; DISTRIBUTION UNLIMITED.

13. SUPPLEMENTARY NOTES

14. ABSTRACT

Results for modeling, simulation, and analysis of interference effects that modern wideband signals have on existing narrowband radar system performance are presented. In particular, radar detection performance is characterized using a basic radar receiver model and operational parameters *consistent* with those of the ARSR-4 air route surveillance radar.

Two modern wideband signals (interferers) are addressed in this work, including the GPS military signal (M-Code signal) and a direct sequence ultra wideband (DS-UWB) waveform meeting outdoor emission restrictions imposed by the Federal Communications Commission (FCC). Interference effects are characterized for an unmodulated sinusoidal pulse, as well as, linear frequency modulated (LFM) and bi-phase Barker coded pulse compression waveforms. Finally, coherent pulse integration is addressed and interference mitigation demonstrated via improved detection performance.

Worst case detection scenarios from the radar's perspective are considered for all cases. M-Code interference results indicate that at proposed received power levels of −160 to −130 dBW, radar detection performance is severely degraded with expected improvement occurring when pulse integration is employed. DS-UWB interference results indicate that at maximum transmit power levels specified by the FCC, the DS-UWB waveform has minimal impact on detection performance for radar receiver/UWB transmitter separation distances beyond 0.5 meters. This separation distance is reduced further when pulse integration is employed.

15. SUBJECT TERMS

Ultra-Wide-Band, Radar Detection, Coexistence, and GPS M-Code

16. SECURITY CLASSIFICATION OF:			17. LIMITATION OF ABSTRACT	18. NUMBER OF PAGES	19a. NAME OF RESPONSIBLE PERSON
a. REPORT	b. ABSTRACT	c. THIS PAGE			Michael A. Temple, Dr., USAF (ENG)
U	U	U	UU	94	**19b. TELEPHONE NUMBER** *(Include area code)* (937) 785-6565, ext 4279; e-mail: Michael.Temple@afit.edu